Measurement of Turbine Engine Transient Airflow in Ground Test Facilities

S. Wehofer
ARO, Inc.
and
R. Rivir
Aero-Propulsion Laboratory,
Wright-Patterson Air Force Base, Ohio

August 1980

Final Report for Period October 1, 1977 – November 30, 1979

Approved for public release; distribution unlimited.

ARNOLD ENGINEERING DEVELOPMENT CENTER
ARNOLD AIR FORCE STATION, TENNESSEE
AIR FORCE SYSTEMS COMMAND
UNITED STATES AIR FORCE

NOTICES

When U. S. Government drawings, specifications, or other data are used for any purpose other than a definitely related Government procurement operation, the Government thereby incurs no responsibility nor any obligation whatsoever, and the fact that the Government may have formulated, furnished, or in any way supplied the said drawings, specifications, or other data, is not to be regarded by implication or otherwise, or in any manner licensing the holder or any other person or corporation, or conveying any rights or permission to manufacture, use, or sell any patented invention that may in any way be related thereto.

Qualified users may obtain copies of this report from the Defense Technical Information Center.

References to named commerical products in this report are not to be considered in any sense as an indorsement of the product by the United States Air Force or the Government.

This report has been reviewed by the Office of Public Affairs (PA) and is releasable to the National Technical Information Service (NTIS). At NTIS, it will be available to the general public, including foreign nations.

APPROVAL STATEMENT

This report has been reviewed and approved.

ROSS G. ROEPKE
Project Manager
Directorate of Technology

Approved for publication:

FOR THE COMMANDER

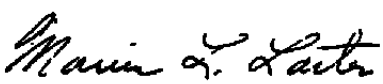

MARION L. LASTER
Director of Technology
Deputy for Operations

REPORT DOCUMENTATION PAGE		READ INSTRUCTIONS BEFORE COMPLETING FORM
1 REPORT NUMBER AEDC-TR-80-21	2 GOVT ACCESSION NO.	3 RECIPIENT'S CATALOG NUMBER
4. TITLE (and Subtitle) MEASUREMENT OF TURBINE ENGINE TRANSIENT AIRFLOW IN GROUND TEST FACILITIES		5 TYPE OF REPORT & PERIOD COVERED Final Report - October 1, 1977, to November 30, 1979 6. PERFORMING ORG REPORT NUMBER
7 AUTHOR(s) S. Wehofer, ARO, Inc., a Sverdrup Corporation Company, and R. Rivir, Aero-Propulsion Laboratory, W-P AFB, Ohio		8 CONTRACT OR GRANT NUMBER(s)
9 PERFORMING ORGANIZATION NAME AND ADDRESS Arnold Engineering Development Center/DOT Air Force Systems Command Arnold Air Force Station, Tennessee 37389		10 PROGRAM ELEMENT PROJECT, TASK AREA & WORK UNIT NUMBERS Program Elements 65807F and 62203F Project 3066, Task 0428
11 CONTROLLING OFFICE NAME AND ADDRESS Arnold Engineering Development Center/DOS Air Force Systems Command Arnold Air Force Station, Tennessee 37389		12 REPORT DATE August 1980 13 NUMBER OF PAGES 75
14 MONITORING AGENCY NAME & ADDRESS(if different from Controlling Office)		15 SECURITY CLASS. (of this report) UNCLASSIFIED 15a. DECLASSIFICATION DOWNGRADING SCHEDULE N/A

16 DISTRIBUTION STATEMENT (of this Report)

Approved for public release; distribution unlimited.

17 DISTRIBUTION STATEMENT (of the abstract entered in Block 20, if different from Report)

18 SUPPLEMENTARY NOTES

Available in Defense Technical Information Center (DTIC)

19 KEY WORDS (Continue on reverse side if necessary and identify by block number)

propulsion system components	transients	subsonic
stability	airflow	venturi
control	measurement	
turbines	simulators	
	jet engine inlets	

20 ABSTRACT (Continue on reverse side if necessary and identify by block number)

Transient airflow is a primary parameter required to evaluate propulsion system component matching, stability and control, and transient engine performance. Development and verification of techniques to calculate turbine engine transient airflow performance have been a difficult, long-term problem. In this study a turbine engine transient airflow simulator was developed and used to evaluate candidate transient airflow measurement

DD FORM 1 JAN 73 1473 EDITION OF 1 NOV 65 IS OBSOLETE

20. ABSTRACT (Continued)

systems. Design criteria and analysis procedures are presented for an engine inlet bellmouth and engine subsonic venturi transient airflow measurement system. The recommended systems have nominal transient airflow measurement uncertainties of 1 percent.

AFSC
Arnold AFS Tenn

PREFACE

The work reported herein was conducted by the Arnold Engineering Development Center (AEDC), Air Force Systems Command (AFSC), and the Aero-Propulsion Laboratory (APL), Wright-Patterson Air Force Base, Ohio. The results of the test were obtained by ARO, Inc., AEDC Division (a Sverdrup Corporation Company), operating contractor for the AEDC, AFSC, Arnold Air Force Station, Tennessee, under ARO Project Number E32H-06. The data analysis was completed on November 30, 1979, and the manuscript submitted for publication on April 11, 1980.

The authors would like to express their appreciation to Mr. E. L. Hively, the Air Force program manager; Mr. J. P. Hodge; instrumentation system engineer; and Mr. M. Simmons, test engineer.

CONTENTS

ILLUSTRATIONS

Figure

Figure

Page

TABLES

APPENDIXES

1.0 INTRODUCTION

Transient airflow is a primary parameter required to evaluate propulsion system component matching, stability and control, and transient engine performance. Development and verification of techniques to calculate turbine engine transient airflow performance have been a difficult, long-term problem. The principal deterrent to a solution has been the lack of a standard transient measurement system to use for evaluating techniques and identifying problem areas. In ground test propulsion facilities, there are basically three airflow metering systems used to evaluate engine transient airflow rates: (1) the sonic venturi, (2) the engine bellmouth, and (3) the engine fan.

In 1961, a sonic venturi steady-state airflow measurement system was developed at the Engine Test Facility (ETF) of the Arnold Engineering Development Center (AEDC) (Fig. 1 and Ref. 1). The venturi is located upstream of the engine plenum because of engine inlet airflow quality conditioning considerations. The sonic venturi system is simple and durable; it requires minimal maintenance and has a potential steady-state airflow measurement uncertainty of less than 0.5 percent. For transient engine operation, the rate of change of the engine airflow is determined by calculating the sonic venturi instantaneous airflow rate and evaluating the flow dynamics of the volume between the venturi throat and engine inlet plane. The isolated sonic venturi transient method has two principal disadvantages: (1) The method requires an accurate determination of test cell volumes and flow density time derivatives, and (2) during transient engine testing, a sonic venturi acts as a flow throttling system, which results in reduced flow control for simulation of transient engine flight conditions.

The second method of estimating engine transient airflow rates involves the engine inlet bellmouth (Fig. 1). The bellmouth is close coupled to the engine inlet; therefore, dynamic volumetric corrections are negligible. The pressure drop across the bellmouth is minimal; thus, the system does not limit flow control capabilities for engine transient flight simulation. However, the steady-state experimental airflow measurement uncertainty of engine inlet bellmouth systems has been from two to four times greater than that of isolated sonic venturi systems. The increased measurement uncertainty can be attributed to errors in the measurement of the bellmouth flow dynamic head. Typically, engine bellmouth Mach numbers range from 0.1 to 0.4; therefore, a small error in measured pressure results in a significant error in calculated flow rate.

The third method of estimating transient airflow is to use a modified steady-state engine fan rotor speed/airflow relationship, for which it is assumed that the transient effects of blade clearance and cooling/heating of the fan blades and vanes can somehow be evaluated,

and that the slope of the corrected fan speed lines on the compressor map has a linear shape. Also, during transient operation of turbofan engines, the fan bypass flow will vary with the transient requirements of the high pressure compressor so that transient bypass airflow correction factors, which are engine peculiar, are required.

In a preliminary study, comparison of the three transient airflow measurement methods was made using J57 turbojet engine data. Two instrumentation schemes were used to evaluate the engine bellmouth technique. The results from the comparison are shown on Fig. 2. There are two points to be made concerning this comparison: (1) There is up to 10-percent variation in the predicted results, and (2) the actual engine transient airflow rate is not known. As a result of this and similar comparisons, a joint effort was undertaken by AEDC and the Air Force Aero-Propulsion Laboratory (AFAPL) to develop a system that (1) simulates engine transient airflow rates to a known uncertainty and (2) can be used to develop an accurate engine transient airflow measurement system. This report describes an engine transient airflow simulator, evaluates engine transient airflow measurement systems, and states airflow quality requirements.

2.0 APPARATUS

2.1 TEST ARTICLES

The test articles for this program consisted of a turbine engine transient airflow simulator and three flow-metering systems — an engine bellmouth, a subsonic venturi, and a sonic venturi.

2.1.1 Turbine Engine Transient Airflow Simulator

A Turbine Engine Transient Airflow Simulator (TETAS) was designed and fabricated at AEDC (Fig. 3). The simulator consists of a bulletnose, support struts, translating plug, and two outer shroud assemblies for two different flow ranges. The inlet diameter and bulletnose geometry correspond to a J85 turbojet engine. The translating plug is actuated by a 2,000-psig hydraulic pressure system with a maximum translation rate of 12 in. per second. The simulator can be used with either a 12- or 6-in. displacement hydraulic cylinder and with two corresponding shroud configurations (Fig. 4). With the 12-in. hydraulic cylinder and shroud configuration A, the simulator has a corrected airflow range of from 20 to 42 lbm per second. With the 6-in. cylinder and shroud configuration B, the corrected airflow range is from 8 to 16 lbm per second. The TETAS has the capability to simulate engine acceleration/deceleration transient airflow rates corresponding to throttle transients from idle to military power in one second. This time exceeds the transient rate capability of current advanced engine control systems by a factor of from two to four.

2.1.2 Airflow Metering Nozzles

The engine inlet bellmouth initially used in the program is shown in Fig. 5. The bellmouth was designed and used for J85 engine sea-level-static testing at Air Force Aero-Propulsion Laboratory (AFAPL). The inlet wall contour corresponds to a 2:1 ellipse; the cylindrical section of the bellmouth has eight instrument portals located in a circumferential plane 1.6 duct radii upstream of the engine face station.

The second metering system was an engine direct-connect subsonic venturi designed and fabricated at AEDC (Fig. 6). The venturi has an ASME low beta inlet wall contour, a short cylindrical throat, a conical diffuser and a flow-straightener section. Two exit-flow-straightener configurations (Fig. 7) were tested.

The third metering system tested was a sonic venturi (Fig. 8) which was designed in accordance with the criteria specified in Ref. 1.

2.2 TEST CELL CONFIGURATIONS

The engine airflow simulator and metering nozzles were installed in the R2A2 Research Propulsion Area in the ETF. Two test cell configurations were used—a conditioned/air inlet configuration (Fig. 9) and an atmospheric air inlet configuration (Fig. 10).

The conditioned air configuration is connected to the ETF airside compressors and the auxiliary air-conditioning equipment. Test cell inlet air pressure is controlled with a 12-in. throttle plug control valve that has a dynamic response rate of two radians per second. Test cell steady-state airflow rates are measured with a sonic venturi (Fig. 8). The venturi inlet flow quality conditioning equipment consists of a honeycomb section, perforated plate, and a flow-straightening grid with a uniform screen overlay. Bellmouth inlet flow quality conditioning equipment consists of a perforated venturi corebreaker plate and a flow-straightener grid with a uniform screen overlay. The expended test airflow is vented to atmosphere through the ETF exhaust compressors.

For atmospheric air inlet testing, an air filter housing is placed in the front of the engine plenum section (Fig. 10). The filter housing had a surface area of about 250 square feet and an inlet air velocity, based on a uniform inlet flow distribution, of from two to three feet per second.

2.3 INSTRUMENTATION

Pressures are measured with bonded resistive strain-gage absolute transducers and piezoresistive strain-gage differential transducers. Temperatures are measured with copper-constantan thermocouples. Voltage outputs from the transducers and thermocouples are recorded on magnetic tape from high-speed analog-to-digital converters and converted to engineering units with an electronic digital computer. Selected channels of pressure and temperature are displayed in the control room for observation during testing.

Air stagnation temperatures are measured with self-aspirated temperature probes of the type described in Ref. 3. The probe is 0.125 in. in diameter and consists of 26-gage thermocouple wire encased in a magnesium oxide jacket with a stainless steel sheath. Air stagnation pressure probes are 0.125 in. in diameter and constructed in accordance with the criteria specified in Ref. 4. Wall static pressure taps are 0.040 in. in diameter (0.080 was used in the engine bellmouth) and are also installed in accordance with the Ref. 4 criteria.

The installation system for close-coupled pressure transducers is shown on Fig. 11. The arrangement includes a three-way air pilot vacuum valve that allows switching the transducer to a reference pressure for online calibration. The valve has a 1.1875-in.-diameter body, is 1.5 in. high, and has a 0.125-in. pipe thread and orifice. A vacuum is applied to the closed side of the valve diaphragm in order to minimize valve leakage.

2.3.1 Turbine Engine Transient Airflow Simulation

Five close-coupled total-pressure probe systems and five self-aspirated temperature probes are installed circumferentially in the TETAS plenum section (Fig. 3). These probes are used to measure the TETAS airflow pressure and temperature. Simulator skin temperatures are measured with thermocouples peened to the back side of the plug and shroud walls and are used to correct flow area for thermal changes. The plug position is measured with a binary coded decimal shaft encoder. A 0.125-in.-diameter steel cable is attached to the aft end of the simulator plug and wound about a spring loaded pulley attached to the encoder shaft.

2.3.2 Airflow Metering Systems

Calculation of airflow rates, using an engine inlet bellmouth, requires the measurement of airflow stagnation pressure and temperature and, to evaluate flow Mach number, the wall static pressure. The bellmouth evaluated in this program is equipped with four four-probe total-pressure and total-temperature rakes. The rakes are circumferentially spaced and the probes located on centroids of equal flow area. Sixteen wall static pressure taps are located

in a circumferential plane one inch upstream of the total-pressure probe tips. The wall static pressure taps and total-pressure probes were connected to 16 individual rapid-response, 0- to 5-psi, piezoresistive, differential pressure transducers. The differential pressure transducers are mounted in an infinite-tube arrangement (Ref. 5) with the ends of the tubes connected to a scanner valve system. An effort was made to size the instrument tubing to the differential transducers in order to achieve a matched pressure response system. To account for thermal changes in bellmouth flow area, two wall surface temperatures are measured.

The required measured parameters for the subsonic venturi are the same as the engine bellmouth, but different instrumentation systems were used. Venturi stagnation flow conditions are measured in the engine plenum section. Eight close-coupled wall static pressure measurements are used to evaluate stagnation pressure, and a six-probe total-temperature rake is used to measure stagnation temperature. Eight close-coupled wall static pressure measurement systems, located in a circumferential plane at the center of the cylindrical throat section, are used to evaluate throat Mach numbers. Two wall surface temperatures are used to account for thermal changes in the throat flow area.

The calculation of transient airflow rates using the sonic venturi requires the measurement of the fluid stagnation pressure, temperature, and, for subsonic operation, the venturi throat wall static pressure. In addition, measurements of the transient pressure and temperature in the engine plenum are required to evaluate the dynamics of the volume between the venturi flow measuring station and the engine inlet plane. The venturi stagnation flow conditions are measured in the venturi plenum, where eight close-coupled wall static pressure measurement systems are used to evaluate stagnation pressure, and a three-probe total-temperature rake is used to measure stagnation temperature. For unchoked venturi operation, four close-coupled wall static pressure throat measurement systems are used to evaluate throat Mach numbers. Two wall surface temperatures are used to account for thermal changes in throat flow area.

2.3.3 Airflow Quality

Airflow quality evaluation consisted of measuring radial total pressure, velocity, and velocity fluctuations at the engine simulator inlet plane. Total pressure is measured with two eight-probe rakes mounted on the TETAS bulletnose struts (Fig. 10). The rake probes are located on centroids of equal area with the outermost probe located at 0.99 of the wall radius. The radial velocity profile and the turbulence profiles are evaluated with a hot-wire traverse system with static pressure measurements on the bulletnose surface and the opposing wall. The traverse system employs a Thermo Systems Model 1052 anemometer, which was operated in the constant-temperature mode with Model 1210 sensor supports. The nominal frequency response for a 4-μm wire diameter is on the order of 25 KHz and

about 12 KHz for a 51-μm-diameter film. The apparent background noise level of the anemometer is maintained at an order of magnitude less than any reported value of the fluctuating component of velocity.

3.0 PROCEDURES

3.1 CALIBRATION

All transducer and system calibrations performed during the test are traceable to the National Bureau of Standards (NBS). Each link in the traceability chain is maintained and documented by the AEDC Standards Laboratory (Ref. 6). Posttest measurement uncertainties for both steady-state and transient parameters are given in Table 1. Procedures for calculating uncertainties are presented in Ref. 7.

3.1.1 Pressure Systems

The pressure transducers used in the Automatic Multiple Pressure Scanning (AMPS) system are calibrated in place before and after each test period by applying multiple pressure levels within the pressure range from 0.5 to 50 psia. Each applied pressure level is measured with a pressure-measuring device calibrated in the Standards Laboratory.

3.1.1.1 Differential Transducers

The pressure measurement system for the piezoresistive strain-gage differential transducers is shown on Fig. 12a. This system was initially used for the engine bellmouth. One side of the transducer was connected to a total-pressure probe and the reference side to a wall static pressure tap. The transducers, however, did not have acceptable measurement accuracy. The principal problems were nonrepeatability and signal drift. The differential transducers were used as low-range absolute transducers and calibrated at short time intervals in order to make them acceptably accurate. This was accomplished by connecting one side of the transducer to a constant reference pressure system; the remaining side of the transducer was close-coupled to the pressure-sensing port. The schematic for the close-coupled differential transducer system is shown in Fig. 12b. The rapid-response differential pressure transducers were calibrated at three-to five-minute intervals to correct for signal drift.

3.1.1.2 Absolute Transducers

The pressure measurement system for the close-coupled strain-gage transducers is shown in Fig. 13. This system was used with both the subsonic and sonic venturis. As noted earlier,

the close-coupled strain-gage transducers are calibrated in place both before and after each test period by applying multiple pressure levels within the pressure range from 8 to 15 psia. During the tests, the close-coupled transducers are in-place calibrated at 15-min intervals. In-place calibration is performed to compensate for transducer drift and to limit bias between the different transducers.

3.1.1.3 Pressure Response Requirements

The estimated frequency response requirements for the engine transient airflow measurement systems are on the order of from 1 to 10 Hz. The required frequency response was determined with use of a pressure response analysis to evaluate difference error between the source and measured pressure time response curves for given close-coupled plumbing configurations (Ref. 8). The frequency response of the proposed plumbing for the differential transducer infinite tube arrangement (Fig. 12a) is estimated — by noting previous experimental results (Ref. 5) — to be from 100 to 300 Hz at the three-decibel point, which is an order of magnitude greater than required. However, there was concern that the infinite tube system would have a mass-transfer lag or capacitance problem since the system might not load or dump line pressure at the same rate as the source pressure.

Tests were conducted to determine the frequency response of the proposed plumbing for the close-coupled pressure transducer system. A pressure pulse generator (Fig. 14) was constructed using a tank for a constant control pressure source. The plumbing of this system allows the transducer to measure the tank pressure when the solenoid is de-energized and the atmospheric pressure when energized. The output of the transducer was recorded on an oscillograph, and pressure pulse rise/decay times were reduced from the oscillograph trace. A similar frequency response test was also conducted with the transducer installed in the test cell using the test cell ducting as the volume tank. The test results show that the close-coupled, absolute pressure system has an average frequency response of 10 Hz at the three-decibel point. The estimated transient measurement uncertainties for the close-coupled pressure system are presented in Table 1.

3.1.2 Temperature Systems

3.1.2.1 Steady-State

Thermocouples were fabricated from wire conforming to the Instrument Society of America specifications. Before and after each test period, known millivolt levels were applied to each temperature recording system. The corresponding temperature equivalents were obtained from 150°F reference tables based on the NBS temperature vs millivolt tables.

Nonlinearity in the thermocouple characteristics was accounted for in the data reduction program.

3.1.2.2 Transients

Estimates of the characteristic time constants for the self-aspirated temperature probes were obtained from data contained in Ref. 9. The estimated reference time constant (τ_o, sec) for this air stagnation-temperature-measurement probe is 0.34. For the range of test conditions, the present air temperature probe time constant can be approximated with

$$\tau = \frac{0.34}{\sqrt{M}}, \text{ sec}$$

For a step fluid temperature change from T_i to T_f, a first-order response equation for a convective and internal energy thermal balance is

$$\frac{T_f - T}{T_f - T_i} = e^{t/\tau}$$

For 95 percent of the temperature step, the self-aspirated probe temperature response rate can be approximated by

$$t = \frac{0.017}{\sqrt{M}}, \text{ sec}$$

3.1.3 Turbine Engine Transient Airflow Simulator

The position indicator for the airflow simulator plug was calibrated in place at selected intervals before each test period. End point calibrations were based on mechanical stops built into the hydraulic displacement cylinders.

The engine airflow simulator was calibrated in the conditioned air inlet test configuration (Fig. 9). A sonic venturi operated in the critical flow mode was used to provide a known airflow rate as a function of simulator plug position. The venturi airflow measurement uncertainty is presented in Table 2. The simulator plug was set at approximately 0.5-in. increments with a range of inlet flow stagnation conditions of from 10 to 15 psia and from

500 to 550°R. The simulator calibration curves were analytically curve fitted with a least-squares, second-order polynomial and were used in the data reduction program. The TETAS transient airflow uncertainty estimates are presented in Table 3.

3.2 AIR PRESSURE CONTROL SYSTEM

During transient testing with the conditioned air inlet test configuration (Fig. 9), an effort was made to maintain the engine plenum pressure constant. The engine plenum pressure was measured with an absolute-pressure transducer and monitored by the ETF plant computer control system, which in turn controlled the inlet air pressure control valve.

3.3 TEST CONDITIONS

Transient airflow calibration data were obtained at nominal sea-level-static conditions with excursion test data for stagnation flow conditions of from 10 to 15 psia and from 500 to 550°R. Test cell airflow rates were varied with use of the TETAS. With the conditioned air test cell configuration (Fig. 9), the airflow rates varied between 8 and 16 lbm/sec. With the atmospheric inlet air test cell configuration (Fig. 10), the airflow rates varied between 20 and 42 lbm/sec. The test airflow rates were varied by translating the TETAS throttling plug, which varies the TETAS flow area. The TETAS exit pressure was kept below three psia so that the TETAS nozzle flow coefficient remained independent of the exhaust pressure. The TETAS throttling plug was actuated at transient rates between 1 and 15 sec, stop to stop.

4.0 RESULTS AND DISCUSSION

The basic assumption made in calculating engine transient airflow rates is that the flow process is quasi-steady. This is justified by the fact that pressure waves travel at acoustic speeds which are much greater than the pressure time transients encountered with engine flow transients. Although temperature transients are controlled by heat transfer processes and, therefore, require much longer equilibrium times than pressure, most engine testing is for constant air temperatures or temperatures that have transient rates of less than 1 to 2°/sec. Therefore, to calculate engine transient airflow rates, flow properties and metering nozzle mass flow coefficients are determined based on measured values for a given time. The cost and operational advantages of theoretically as opposed to experimentally derived flow coefficients are obvious, and ETF has shown (Refs. 1, 10, 13, and 14) that accurate theoretical values can be obtained. Use of theoretical coefficients, however, requires that the metering nozzle flow process be consistent with the analytical assumptions. This generally requires that the flow be two-dimensional, adiabatic, and free of large flow disturbances

such as can occur as the result of instrument rakes or an engine bulletnose in close proximity to the airflow measuring station. Analyses (e.g., Ref. 11) can be used to predict the effect of nonadiabatic flow on wall boundary layers, but these types of analyses have not received the same degree of experimental verification as adiabatic flow analysis. Further evaluation is required before theoretical flow coefficients can be used for flows having large temperature changes in short time periods.

4.1 ENGINE BELLMOUTH

The existing J85 engine bellmouth (Fig. 5) with differential pressure transducers (Fig. 12a) was the first system tested. The bellmouth instrumentation system is described in Sections 2.3.2 and 3.1.1.1. The bellmouth steady-state flow coefficients (Fig. 16) were evaluated in the conditioned air inlet test installation (Fig. 9). There are three points to be made concerning the calibrated flow coefficients. Normally, flow coefficients are plotted as a function of Reynolds number, but Fig. 16 illustrates how data scatter and measurement uncertainty decrease with increasing flow Mach numbers. This results from the improved measurement accuracy with the increase in the flow dynamic pressure differential. That the mean data flow coefficient curve fit has a value greater than unity is the result of the instrument rake aerodynamic blockage and the oversized (0.080-in.) wall static pressure taps. Finally, it should be noted that the estimated measurement uncertainty for this system is considered unacceptable for engine testing.

The bellmouth measurement uncertainty can be improved by using the differential pressure transducers as low-range absolute transducers as discussed in Section 3.1.1.1. An estimate of the bellmouth transient airflow measurement uncertainty that can be expected as a result of using different instrumentation schemes is presented in Fig. 17. The estimates are based on bellmouth flow coefficients obtained from steady-state calibration which used a transient instrumentation system, and a sonic airflow metering venturi, and an online pressure calibrator system. Figure 17 shows that if the region of interest is less than a flow Mach number of 0.3, then the differential pressure measurement system that is used as a low-range absolute transducer with an online calibration system should be selected. For flow Mach numbers greater than 0.3, an absolute strain-gage transducer with an online calibration system should be selected. For flow Mach numbers greater than 0.6, the absolute-pressure transducer system with a resistance calibration system provides uncertainties of approximately one percent without the mechanical and operational complexities of an online pressure calibration system. Transient airflow data are presented in Section 4.2.2 that substantiate the measurement uncertainty estimates shown in Fig. 17.

4.2 SUBSONIC VENTURI

4.2.1 Design Considerations

Engine face Mach numbers generally range from 0.1 to 0.4; the transient airflow measurement uncertainty using a bellmouth measurement system for this level of Mach number may be unacceptable (Fig. 17). Increasing the flow Mach number by reducing the flow area is one way to improve the airflow measurement uncertainty. In this report, an engine bellmouth having a flow measuring station with a diameter less than the engine inlet diameter is referred to as a subsonic venturi. A subsonic venturi has a greater Mach number in the venturi throat section than does an engine bellmouth for a given engine face Mach number. Designing a subsonic venturi requires consideration of the inlet contour, throat region, and exit contour. The venturi inlet and throat geometry must be evaluated for the effects of (1) the sensitivity of throat static pressure tap location on airflow measurement uncertainty, (2) the mass-flow coefficient for streamline curvature and boundary-layer displacement, and (3) the contour requirements to provide a prescribed throat flow field and Mach number.

The venturi exit section must be evaluated for (1) pressure recovery characteristics and (2) radial pressure distortion.

4.2.2 Design Recommendations

The proposed design for the subsonic venturi is the result of a design study that included evaluating several geometry concepts and various aerodynamic factors. Experimental data and ETF nozzle and boundary-layer computer codes (Refs. 10, 11, and 12) were used to evaluate the various venturi geometry configurations. The subsonic venturi design that resulted from this study is shown in Fig. 6. The venturi was designed with a cylindrical throat with a length of from one to two throat radii. Static pressure measurement in a cylindrical throat section is not highly sensitive to throat static pressure tap location, whereas it is very difficult to locate static taps at precisely the aerodynamic minimum area of a continuous-contour, single-plane-throat venturi. In the prescribed cylindrical throat section, the static pressure taps can be placed within $\pm 0.1R^*$ of the midpoint with less than 0.1-percent error in mass flow. The venturi inlet contour corresponds to that for a low beta airflow metering nozzle, as recommended by the American Society of Mechanical Engineers (ASME) (Ref. 2). For flow Mach numbers less than 0.7, the streamline curvature flow coefficient for this inlet contour can be considered unity, and the wall boundary-layer displacement determines the venturi mass-flow coefficient which, in general, will be a value greater than 0.99. This particular venturi configuration can be used for throat Mach numbers of up to

approximately 0.8 before encountering local supersonic flow accelerations at the inlet transitional section. Local supersonic bubbles and shocks, at high subsonic throat Mach numbers, would preclude an accurate theoretical evaluation of the nozzle flow coefficient.

A gradual wall contour is used at the exit of the cylindrical throat section to avoid local flow separation or large flow disturbances that feed back to the flow measuring station. The selection of a 12-deg included-angle, divergent-diffuser section is based on ETF subsonic flow operational experience with sonic type venturis. Flow-straightening equipment usually will be required to meet engine face airflow quality requirements. The pressure recovery and radial pressure distortion of the subsonic diffuser exit flow are a function of the venturi throat Mach number which, in turn, is a function of the pressure drop across the exit-flow-straightener screens. Final design criteria for subsonic venturi flow-straightening equipment have not yet been established and, as with all hardware of this type, will be developed with operational experience. ETF has considerable experience in designing engine bellmouth flow-straightener and flow-distortion screens, and, in almost every case, cold-flow calibration tests are required to finalize the screen patterns. Appendix A presents a procedure for estimating flow-screen pressure-drop flow characteristics required to size the venturi throat diameter, and Appendix C presents criteria to initiate the flow straightener design.

4.2.3 Airflow Metering Performance

A subsonic venturi was designed in accordance with the design criteria specified by Fig. 6 and contained in Appendix A. The venturi was sized to have a throat Mach number range of from 0.26 to 0.65 for an air stagnation pressure of 14 psia and temperature of 520°R. This Mach number range corresponds, for the same corrected airflow rates, to an engine face Mach number range of 0.15 to 0.4. The venturi inlet diameter was 25 in. and a minimum length cylindrical throat of 6.3 in. (R*) was used. The exit-flow-straightener screen (Fig. 7a) was designed for an estimated flow blockage of 48 percent (Appendix A). The venturi was calibrated for steady-state flow coefficients in the conditioned air inlet installation (Fig. 9). The venturi instrument system and calibration procedures are described in Sections 2.3 and 3.1.1.2. A comparison of the venturi steady flow results (Fig. 18) with the bellmouth calibration data (Fig. 16) shows that the increased Mach number and improved instrumentation system significantly reduce the data scatter and reduce the flow coefficient to a value between 0.99 and unity. A comparison of theoretically predicted flow coefficients and the mean curve fit through the calibration data is made on Fig. 19. The theoretical flow coefficients were evaluated using Tucker's analysis (Ref. 12) and the ICRPG turbulent boundary-layer analysis (Ref. 11). These particular analyses were selected because ETF has experimentally verified the theoretical results from these analyses for this type of application

(e.g., Refs. 1 and 14). The Reynolds number used for Fig. 19 is based on the venturi throat diameter and the stagnation flow conditions at the venturi throat section. This form of the Reynolds number is selected to conform with current recommended ASME practices (Ref. 2). The maximum difference between the ICRPG theoretical data curve and the calibration data curve is 0.25 percent and less than 0.1 percent using Tucker's analysis, compared to an estimated nominal 0.5 percent measurement uncertainty band for the calibrated flow coefficients.

The venturi was evaluated transiently in the atmospheric inlet installation (Fig. 10). The experimental apparatus and procedures are described in Sections 2.2, 2.3, and 3.1. Both experimental and theoretically derived steady-state flow coefficients were used to predict the transient airflow data. The ICRPG theoretical curve was used for the theoretical evaluation because it has the maximum deviation from the calibration data curve (i.e., worst case). Typical experimental results are presented in Figs. 20 and 21. Airflow acceleration and deceleration transients of 1, 6, and 12 sec corresponding to engine power transients from near idle to military settings were simulated. The figures include the variation in the airflow pressure with time. The experimental venturi throat Mach number range was from 0.28 to 0.60, which is less than the design range of 0.26 to 0.65; the reason for this difference is that the exit-flow-screen pressure drop was greater than was estimated (Appendix A). The estimated transient airflow measurement uncertainties for Mach numbers of 0.28 and 0.60 are 1.9 and 0.7 percent, respectively (Fig. 17). Figures 20 and 21 include the percent of airflow deviation between calculated transient airflow rates made with calibrated and theoretically derived flow coefficients and the TETAS measured transient airflow rates. The transient airflow measurement uncertainty band for the TETAS is nominally 0.5 percent for the maximum airflow rates and one percent for the minimum airflow rates (Fig. 15). It can be seen that both of the calculated transient airflow rates are within the TETAS measurement uncertainty band. It would appear, therefore, that the estimated airflow uncertainty (Fig. 17) may be overly pessimistic at the lower Mach numbers; with the online calibration strain-gage instrument system, transient airflow measurement uncertainties of approximately one percent can be achieved for throat Mach numbers as low as 0.25 to 0.3. [The percent deviation in airflow is not zero at time zero (see Figs. 20b and 21b) because of the airflow measurement uncertainty difference between the calculated values.]

As a result of the subsonic venturi design study and the analysis of the venturi transient airflow test data, an engine bellmouth design study was conducted. The bellmouth inlet and throat geometry was evaluated according to the same design considerations as were applied to the subsonic venturi. The results of this evaluation in the form of a recommended engine bellmouth design are shown on Fig. 22. The inlet contour corresponds to an ASME recommended low-beta contour. The instrumentation consists of eight equally spaced circumferential wall static pressure taps located 1.2R* downstream of the inlet transition

section (ASME recommendation, see Ref. 2) and a minimum of three duct radii upstream of the engine bullet-nose. The distance of three radii is based on ETF operational experience; a shorter distance requires an evaluation of the flow radial static-pressure gradient at the airflow measuring station. Two bellmouth skin thermocouples spaced 180 deg apart are located at the airflow metering station. This design should not require exit airflow conditioning equipment. Note that the airflow analysis procedures to be used will be the same as used for the subsonic venturi.

4.3 SONIC VENTURI

Sonic venturis (Fig. 8) were developed to meet steady-state airflow measurement requirements of turbine engines (Ref. 1); with proper considerations, these venturis can be used to estimate transient airflow rates. The usual sonic venturi test installation is depicted in Fig. 1. With this type of installation, engine transient airflow rates are determined by calculating the venturi instantaneous airflow rate and evaluating the flow dynamics of the engine plenum volume. For transient engine operation, the sonic venturi are generally required to operate with subcritical flow in order to adequately control engine face pressure during the flow transients. Sonic venturis, as their name implies, are designed for critical flow at the throat; the wall contour is not optimum for subcritical operation (Ref. 13). The most serious problem lies in ascertaining the static pressure tap axial location with respect to the venturi aerodynamic minimum flow area as a function of the venturi flow conditions. Furthermore, the extremely steep pressure gradients in the throat section can cause differences between measured and actual throat static pressures. Many of the venturi subcritical flow problems can be reduced by calibrating the sonic venturi for subcritical operation.

For this study, theoretical flow coefficients were used to calculate the sonic venturi transient airflow rates. The theoretical sonic venturi throat flow coefficient accounts for flow defects resulting from centrifugal forces that produce radial flow gradients and for wall boundary-layer displacement thickness. Figure 23 presents the sonic venturi discharge, curvature, and boundary-layer flow coefficients for atmospheric inlet flow. The curvature flow coefficient was calculated according to the analysis described in Ref. 10, and the boundary-layer displacement flow coefficient was derived by using the analysis described in Ref. 12. The venturi flow discharge coefficient is the product of the curvature and boundary-layer flow coefficients.

4.3.1 Airflow Metering Performance

For this study, a sonic venturi designed to meet the criteria specified in Ref. 1 was used. The venturi was installed in the conditioned air inlet installation (Fig. 9). The venturi

instrument system and calibration procedures are described in Sections 2.3 and 3.1.1.2. During transient flow testing, the venturi had a throat nominal Mach number range of from 0.6 to 1.0. A comparison was made of the transient pressures at instrument stations 2A, 2B, and 2D (Fig. 9). No axial pressure response lags in total pressure were found. The wall static pressure at instrument station 2B was used to evaluate the flow dynamics of the plenum volume. The ratio of the plenum volume to the venturi flow area was representative of ETF cells. Typical transient experimental results are presented in Figs. 24 and 25. Airflow acceleration and deceleration transients of from 1 to 2 and 6 sec, corresponding to engine power transients from near idle to military settings, were simulated. The figures show the time variation in venturi and engine plenum pressure and engine plenum temperature. Time variations of pressure and temperature for the sonic venturi tests were severer than experienced in the subsonic venturi experiments. The variations occur because the test cell airside control system cannot rapidly adjust flow conditions to the TETAS area transient rates. The plenum flow variations do not significantly affect the accuracy of the evaluation of the sonic venturi airflow rates. The flow variations do, however, have a significant effect on evaluation of the engine plenum volumetric dynamic correction because this evaluation requires the engine plenum density-time derivatives. The volumetric dynamic correction calculation is given by

$$DELW = \frac{Vol}{RG\,(T2B)^2}\left[T2B\,\frac{\partial PS2B}{\partial t} - PS2B\,\frac{\partial T2B}{\partial t}\right]$$

where

DELW = delta change in mass flow rate
∂t = time increment for data averaging
∂PS2B = change in static pressure at station 2B for ∂t
∂T2B = change in total temperature at station 2B for ∂t

Figures 24b and 25b present the ratio of the volumetric mass flow correction to the total airflow rate. For the present test configuration, the volumetric correction term was generally between 4 and 6 percent with extremes of as much as 20 percent. The percent airflow deviation between the calculated sonic venturi and TETAS transient airflow rates (Figs. 24b and 25b) were generally between 2 and 3 percent, with some deviations as great as 8 percent. [Again, the percent deviation in airflow is not zero at time zero because of the airflow measurement uncertainty difference in the calculated values.] The mass flow comparison deviations at times other than zero are the result of incongruous calculated flow density-time derivatives. Flow derivatives were calculated by evaluating the difference in flow properties averaged over a time increment of 0.1 sec. Either averaging flow density for a given time increment and calculating density-time derivatives or averaging flow temperature and pressure for a given time increment, determining time derivatives, and then combining to determine density-time derivatives produced no difference or measurement uncertainty improvement in the volumetric correction term.

Figure 26 shows the effect of using different flow-averaging time increments on the volumetric correction mass flow rate. There is very little difference between the results obtained by using the 0.05- and the 0.10-sec time increments, but there is considerable difference when the 0.50-sec time increment is used. Time increments of less than 0.05 sec could not be used because the measurement uncertainty of the parameter was beginning to approach the same order as the difference used to evaluate the derivative. When time-averaging increments of 0.1 or 0.05 sec are used, an accurate determination of density-time derivatives cannot be made for flow pressure spikes. For test conditions with more gradual changes in plenum pressure, the sonic venturi transient airflow deviation is within the transient airflow measurement uncertainty of the TETAS (Fig. 27). To conclude, while the sonic venturi method can be used to evaluate transient airflow rates, there appears to be no advantage of using this method compared to bellmouth or subsonic venturi methods.

4.4 FLOW QUALITY

Flow-metering systems require flow-conditioning equipment at the inlet and, in many cases, at the exit of the system. Inlet flow-conditioning equipment is required to ensure that there are no significant nonaxial velocity components of radial distortion in flow properties. Such equipment is mandatory if theoretical flow coefficients are to be used. Exit flow-conditioning equipment is required to meet downstream engine face airflow quality requirements. [Inlet flow-conditioning requirements are discussed in Appendix B and exit flow-conditioning requirements in Appendix C.]

5.0 SUMMARY OF RESULTS

Design criteria have been established for an engine inlet bellmouth transient airflow measurement system which have an estimated measurement uncertainty of 1 percent for engine face flow Mach numbers greater than 0.25 to 0.3. To achieve this accuracy, a close-coupled, strain-gage absolute pressure transducer and online pressure calibration system are required. The pressure instrument system must be calibrated either at short time intervals or before each data point.

Design criteria have been established for a direct-connect subsonic venturi transient airflow measurement system. The principle of the subsonic venturi is to increase the engine bellmouth flow Mach number at the airflow measuring station; this improves the airflow measurement uncertainty. The subsonic venturi system has the same calculated measurement uncertainty envelope with Mach number as does the recommended bellmouth system; however, the subsonic venturi system provides a higher accuracy at the same engine

face flow Mach number. A subsonic venturi does require exit flow-conditioning equipment. Guidelines are provided for designing both the venturi and the flow-conditioning equipment.

Analyses and procedures are presented that enable a sonic venturi isolated from the engine inlet to be used to measure engine transient airflow rates. The measurement uncertainty that can be achieved depends on the accuracy that can be achieved in evaluating test cell volumes, test cell volume flow density-time derivatives, and venturi subsonic flow coefficients. For tests having small engine plenum density-time derivatives and with a venturi system calibrated for subsonic flow, transient airflow measurements of from 1 to 2 percent are obtainable.

6.0 RECOMMENDATIONS

The following recommendations are made in regard to measuring turbine engine transient airflow rates during tests of airbreathing propulsion systems:

1. For minimal transient airflow measurement uncertainty, the recommended subsonic venturi airflow metering system should be used. The measurement uncertainty is a function of the engine face Mach number — 1.0 to 0.7 percent of reading for engine face flow Mach number variations of 0.15 to 0.5, respectively.

2. The recommended engine bellmouth airflow metering systems should be used for those installations that do not require minimal airflow measurement uncertainty. The transient airflow measurement uncertainty is from 4.0 to 0.8 percent of reading for an engine face flow Mach number variation of from 0.15 to 0.5, respectively.

3. The airflow pressure measurement system used for the airflow metering system should consist of a close-coupled, strain-gage, absolute pressure transducer system with an online pressure calibration system and calibration prior to each data point.

4. The airflow temperature measurement system used for the airflow metering system should have a first-order temperature response rate an order of magnitude less than the measured fluid temperature transients. The system used for the present study consisted of self-aspirated temperature probes using 26-gage copper-constantan calibrated thermocouple wire. A millivolt substitution is used for pretest and posttest calibration.

REFERENCES

1. Smith, Robert E., Jr., and Matz, Roy J. "A Theoretical Method of Determining Discharge Coefficients for Venturis Operating at Critical Flow Conditions." *Transactions of the ASME, Journal of Basic Engineering*, Series D, Vol. 84, No. 4, December 1962, pp. 434-446.

2. American Society of Mechanical Engineers. *Supplement to Power Test Codes.* "Chapter 4: Flow Measurement, Part 5: Measurement of Quantity of Materials." ASME, April 1959.

3. Glawe, George E., Simmons, Frederick S., and Stickney, Truman M. "Radiation and Recovery Corrections and Time Constants of Several Chromel-Alumel Thermocouple Probes in High-Temperature, High-Velocity Gas Streams." NACA TN 3766, October 1956.

4. Pankhurst, R. C. and Holder, D. W. *Wind-Tunnel Technique: An Account of Experimental Methods in Low- and High-Speed Wind Tunnels.* Pitman, London, 1952.

5. Thomson, T. B. "The Effect of Tubing on Dynamic Pressure Recording." Rocketdyne TR 61-3. Presented at the 10th JANAF Solid Propellant Static Test Panel Meeting, Waco, Texas, October 18 — 20, 1961.

6. Owens, C. L. "Calibration Capabilities of the ESF Instrument Branch." AEDC-TR-67-18 (AD648707), March 1967.

7. Abernethy, R. B. et al. (Pratt and Whitney Aircraft) and Thompson, J. W., Jr. (ARO, Inc.). "Handbook Uncertainty in Gas Turbine Measurements." AEDC-TR-73-5 (AD755356), February 1973.

8. Bauer, Robert C. "A Method of Calculating the Response Time of Pressure Measuring Systems." AEDC-TR-56-7 (AD98978), November 1956.

9. Glawe, George E., Holanda, Raymond, and Krause, Lloyd N. "Recovery and Radiation Corrections and Time Constants of Several Sizes of Shielded and Unshielded Thermocouple Probes for Measuring Gas Temperature." NASA TP 1099, January 1978.

10. Wehofer, S. and Moger, W. C. "Analysis and Computer Program for Evaluation of Airbreathing Propulsion Exhaust Nozzle Performance." AEDC-TR-73-29 (AD760541), May 1973.

11. Weingold, H. D. "The ICRPG Turbulent Boundary Layer Reference Program." Pratt and Whitney Aircraft, July 1968.

12. Tucker, Maurice. "Approximate Calculation of Turbulent Boundary Layer Development in Compressible Flow." NACA TN 2337, April 1951.

13. Smith, R. E., Jr., and Wolff, H. E. "Accurate Measurement of Airflow Rate During Tests of Air-Breathing Propulsion Systems." AEDC-TR-68-22 (AD828777), March 1968.

14. Smith, R. E., Jr., and Matz, R. J. "Performance Characteristics of an 8-in.-Dia ASME Nozzle Operating at Compressible and Incompressible Conditions." *Transactions of the ASME, Journal of Fluids Engineering*, Series I, Vol. 95, No. 4, December 1973, pp. 542-550.

15. Pinker, R. A. and Herbert, M. V. "Pressure Loss Associated with Compressible Flow Through Square-Mesh Wire Gauzes." *Journal of Mechanical Engineering Science*, Vol. 9, No. 1, February 1967, pp. 11-23.

16. Faehl, K. C. and Harper, R. E. "Calibration of a J75-P-9 Turbojet Engine at the Sea-Level and Altitude Guarantee Conditions." AEDC-TN-58-55 (AD301602), October 1958.

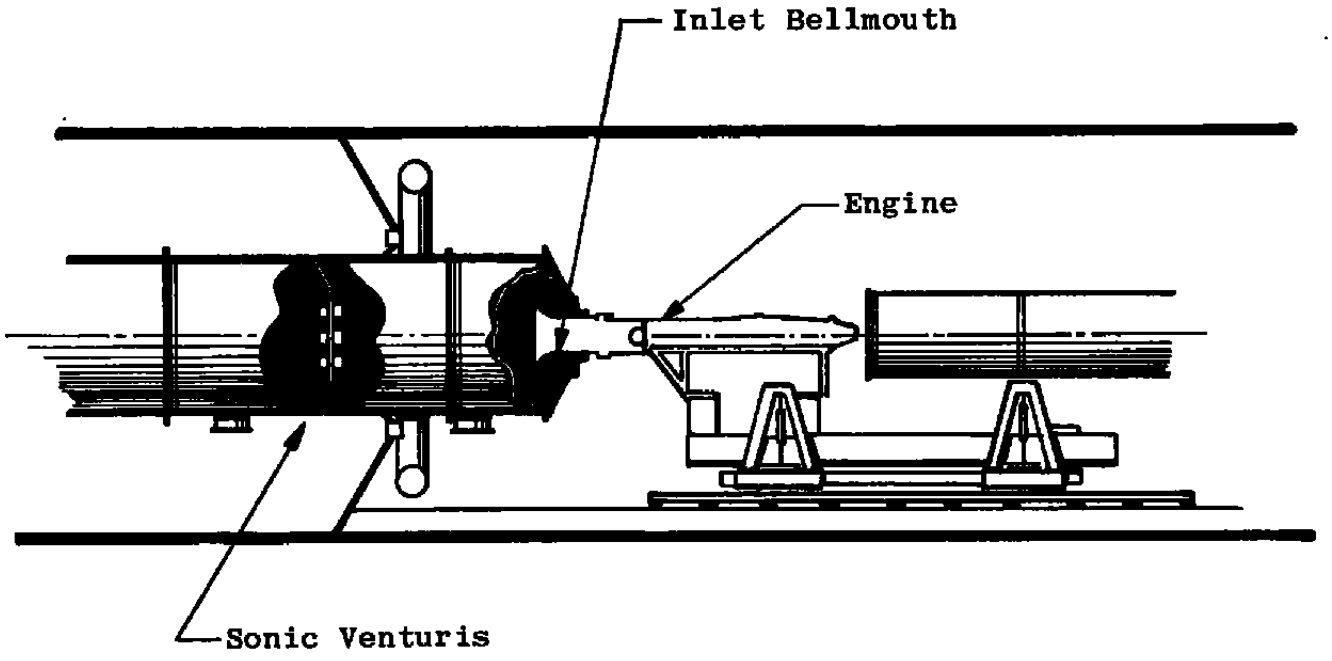

Figure 1. Direct-connect turbine engine test cell installation.

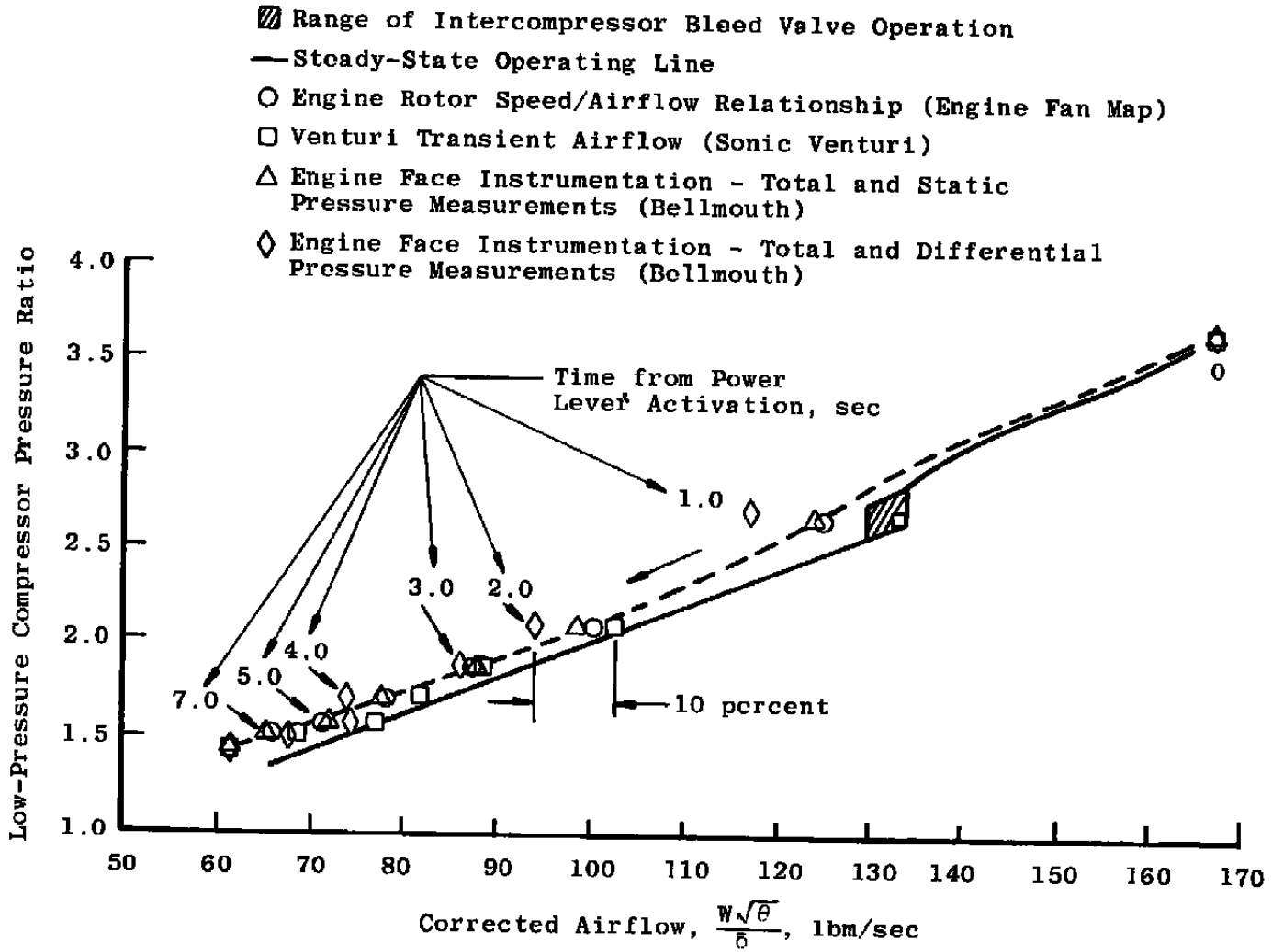

Figure 2. Comparison of airflow measurement techniques during an engine deceleration.

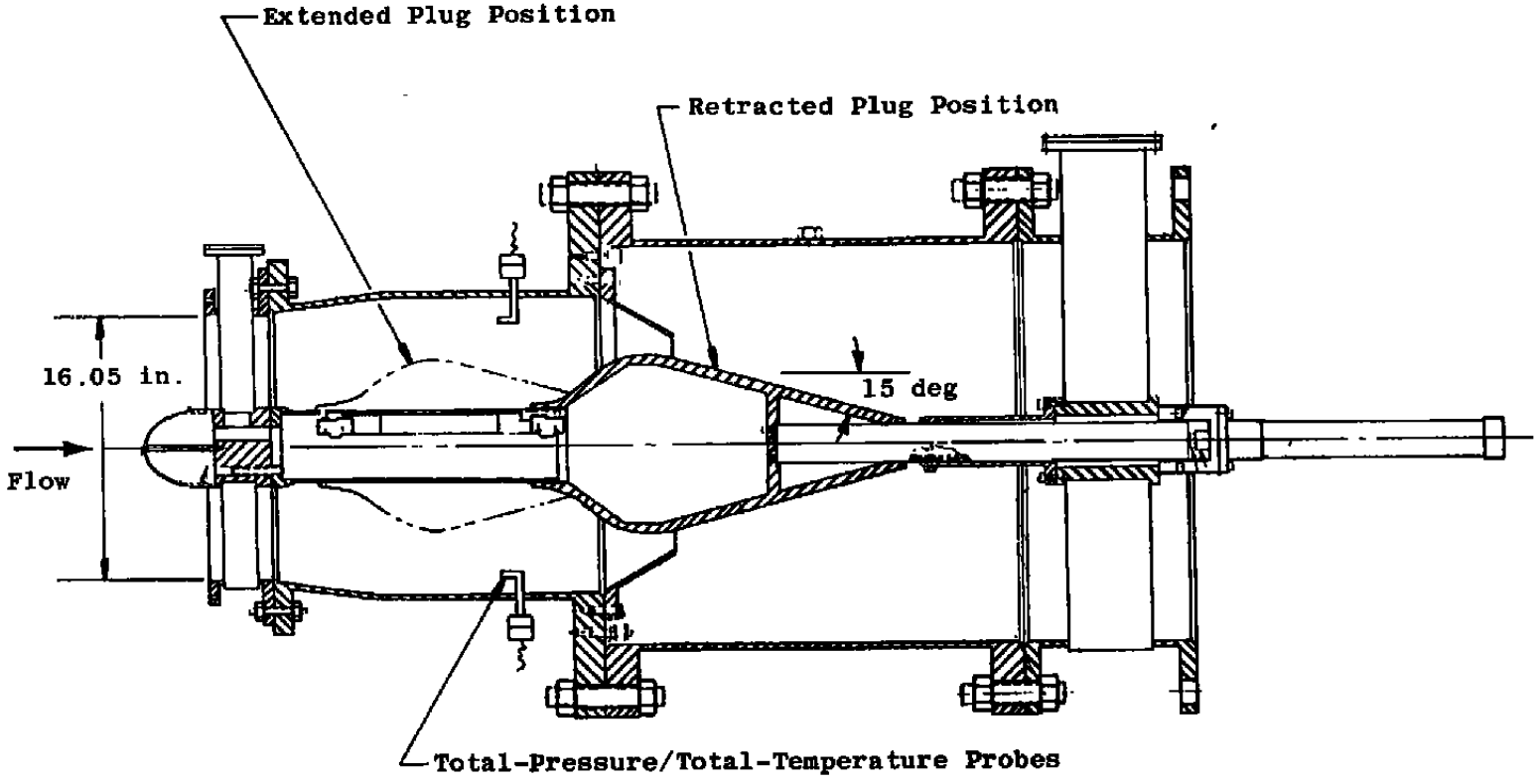

Figure 3. Turbine engine transient airflow simulator (TETAS).

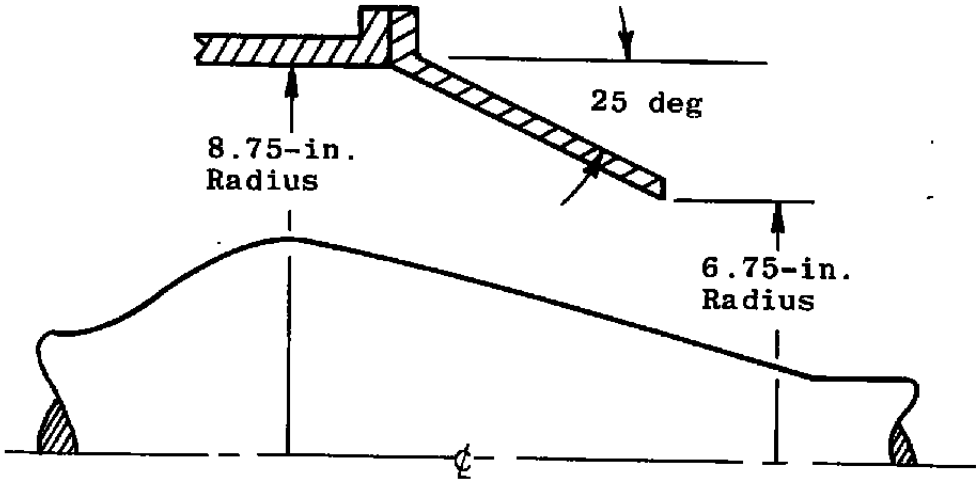

a. Configuration A

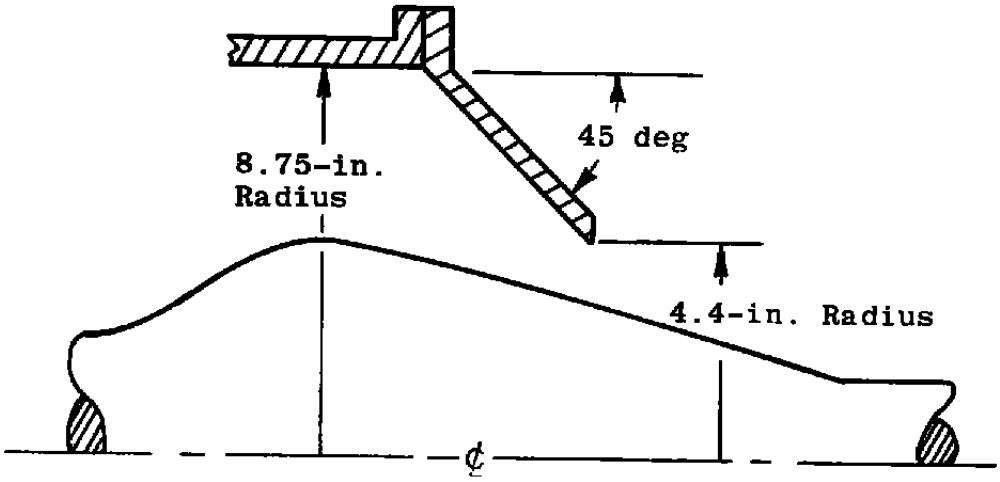

b. Configuration B

Figure 4. Turbine engine transient airflow simulator (TETAS) shroud configurations.

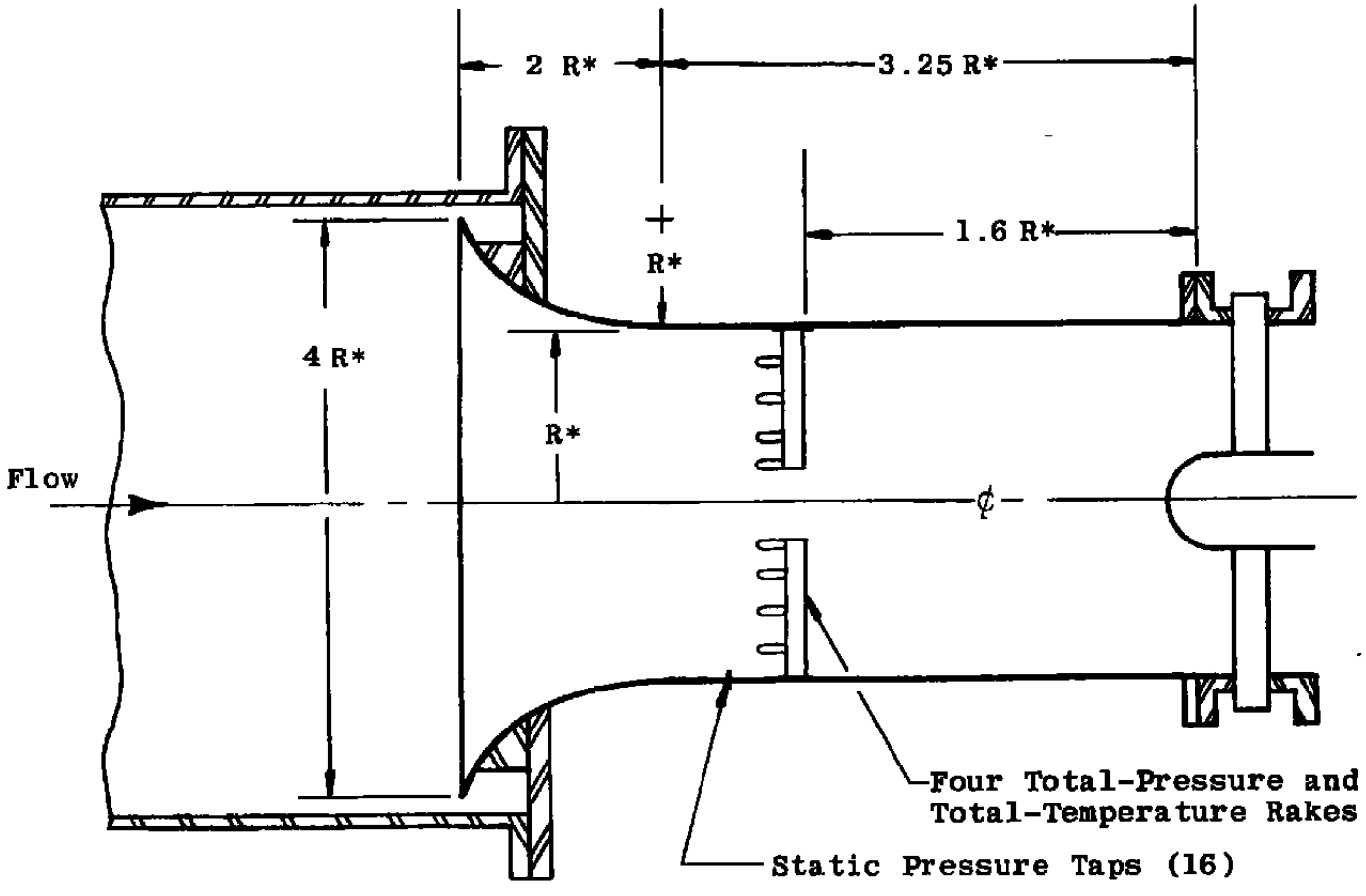

Figure 5. Schematic of a J85 engine inlet bellmouth.

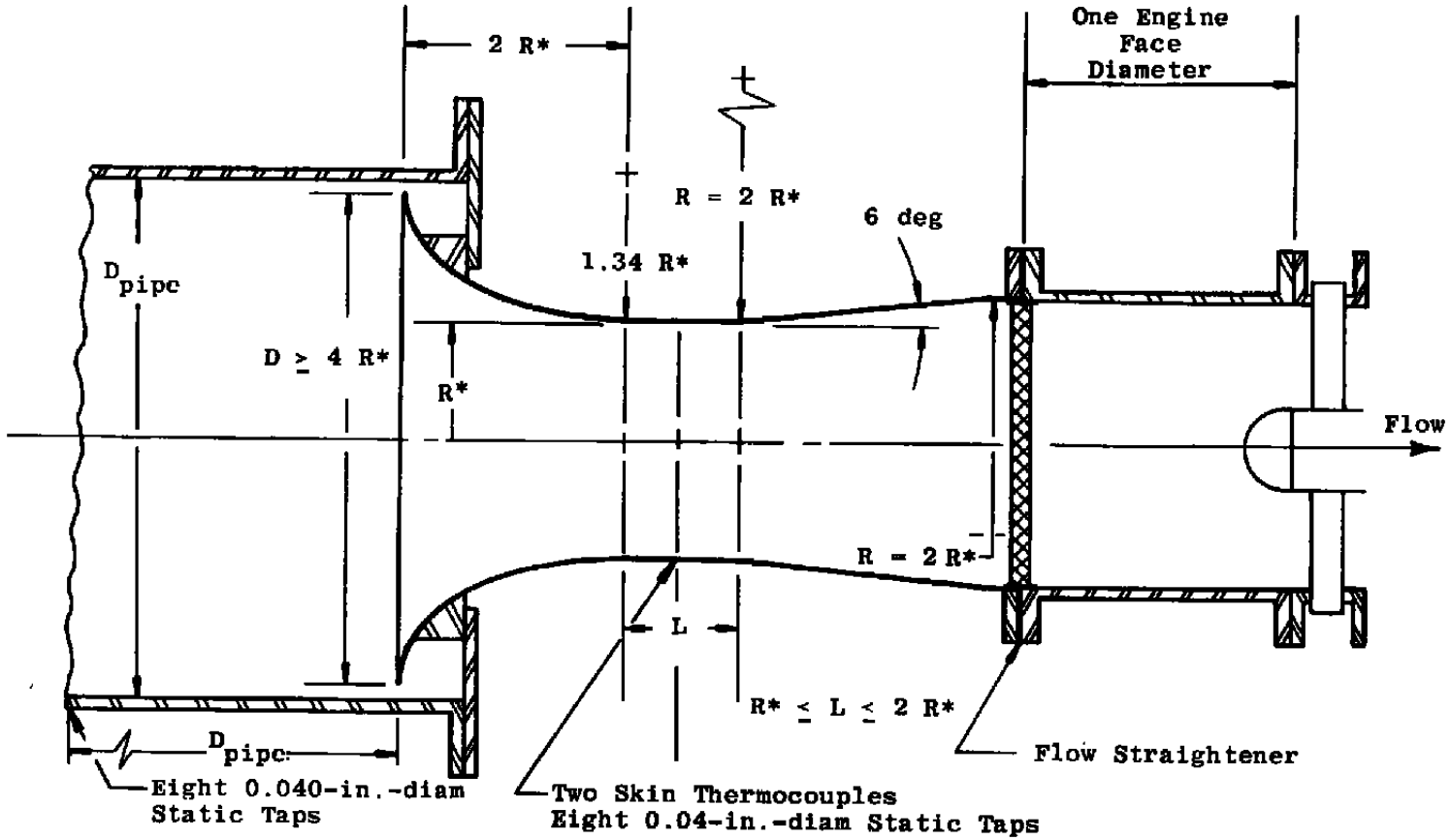

Figure 6. Recommended direct-connect subsonic venturi design.

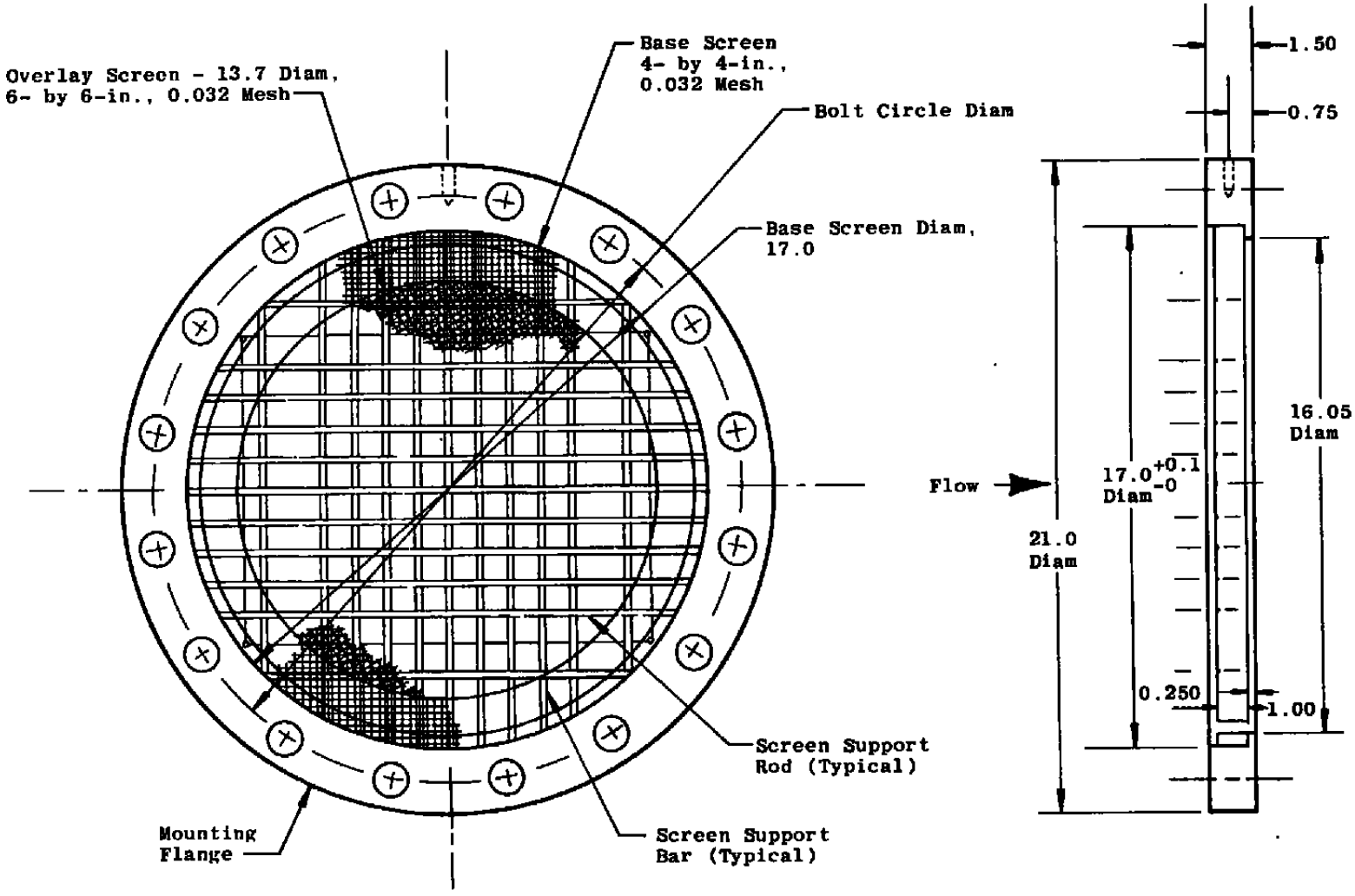

a. Screen Configuration A

Figure 7. Subsonic venturi flow straighteners.

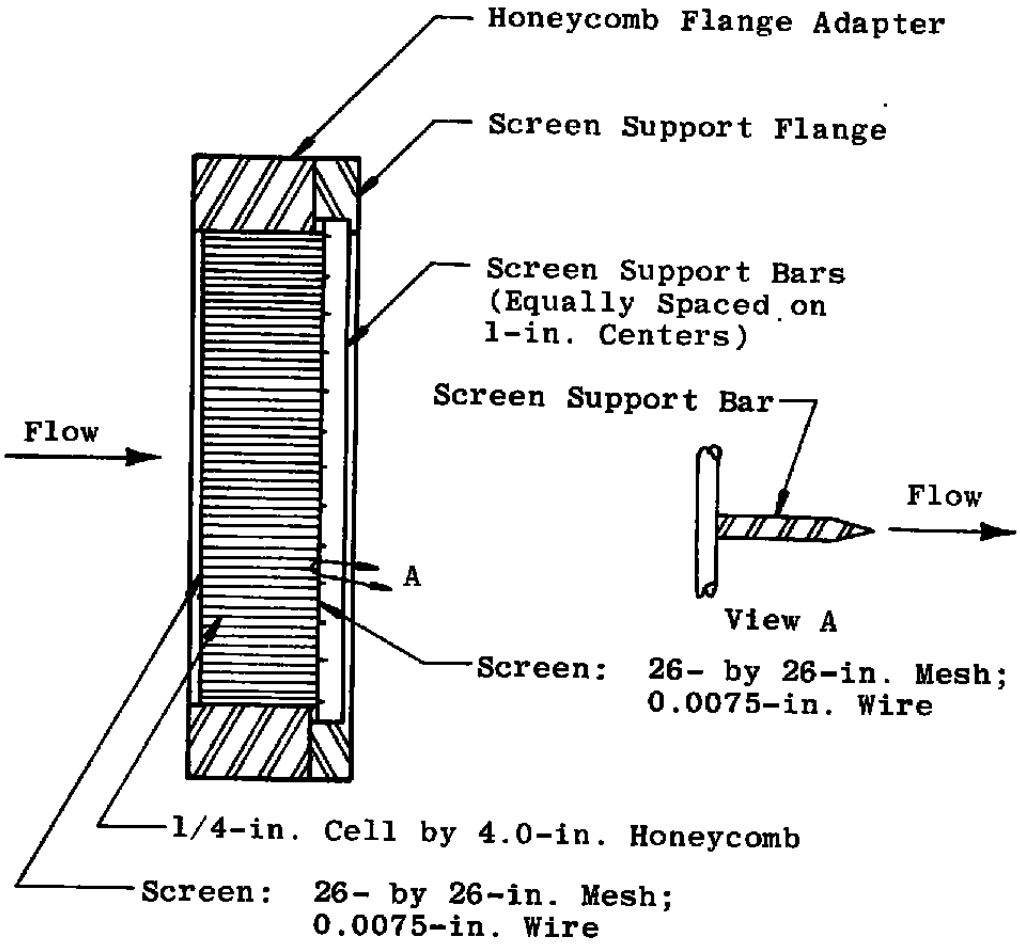

b. Screen Configuration B
Figure 7. Concluded.

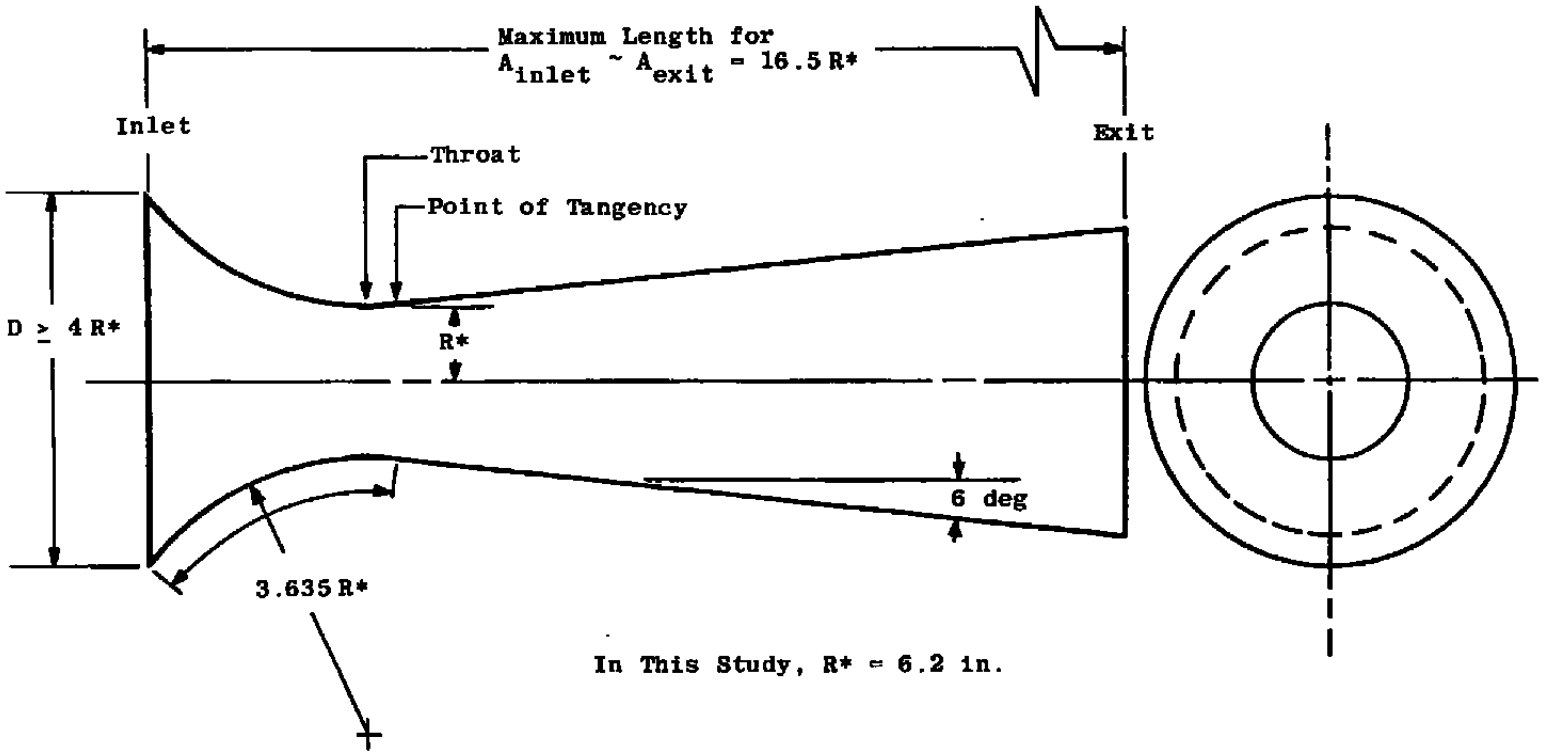

Figure 8. Sonic venturi.

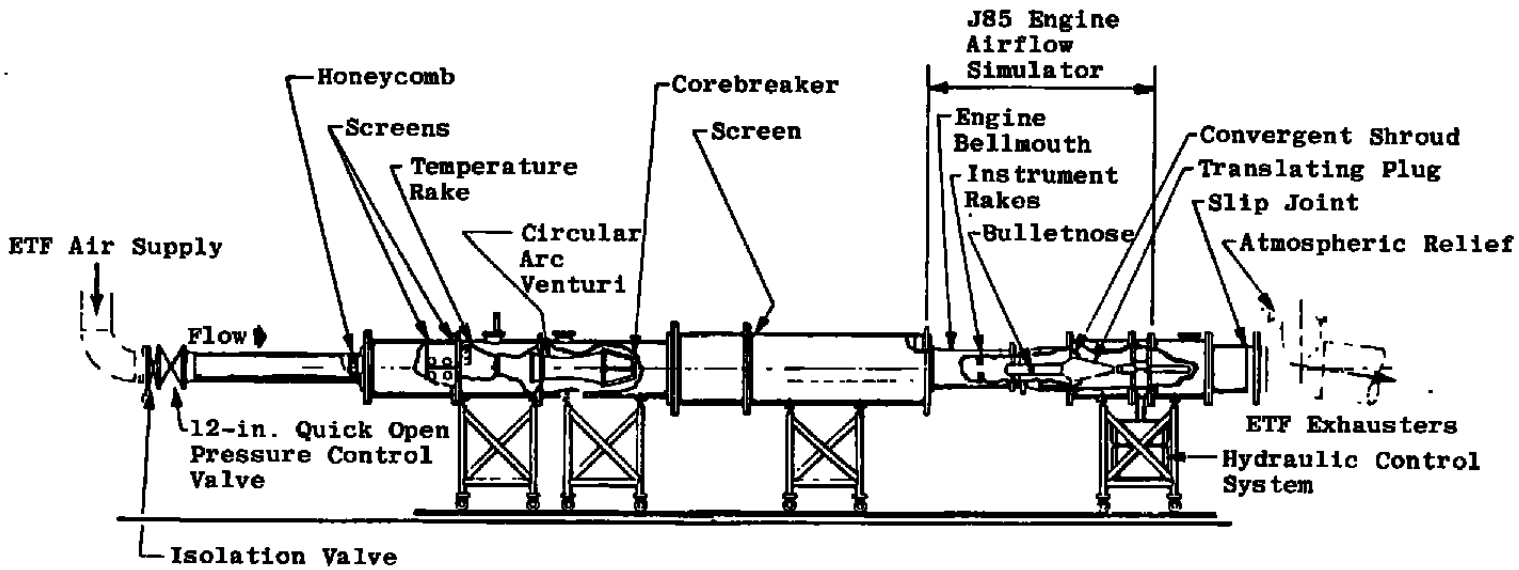

a. Hardware

Figure 9. Test installation – conditioned air inlet.

Measurements	Station Identification														
	-1	ϕ	1A	1B	1C	1D	1E	2A	2B	2C	2D	2E	3A	3B	3C
Total Pressure										16*	16	5			
Static Pressure (Wall)	2	2	2	2		8	4	2	8	16*/8	2		2	4	2
Total Temperature	2				3				6	16*		5			
Skin Temperature							2			2			4		

*Used Only for J85 Engine Bellmouth

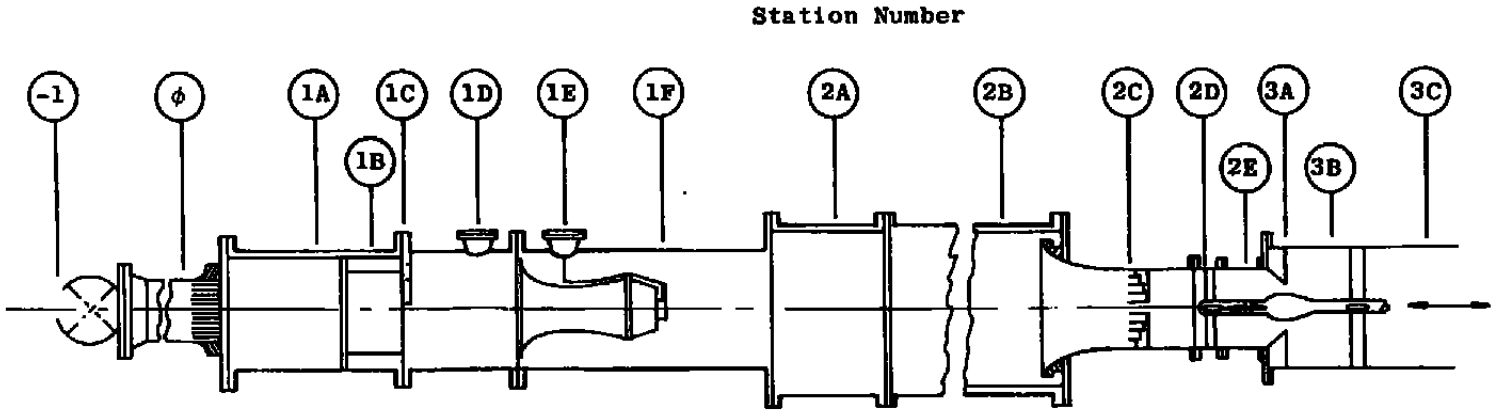

b. Instrument station identification

Figure 9. Concluded.

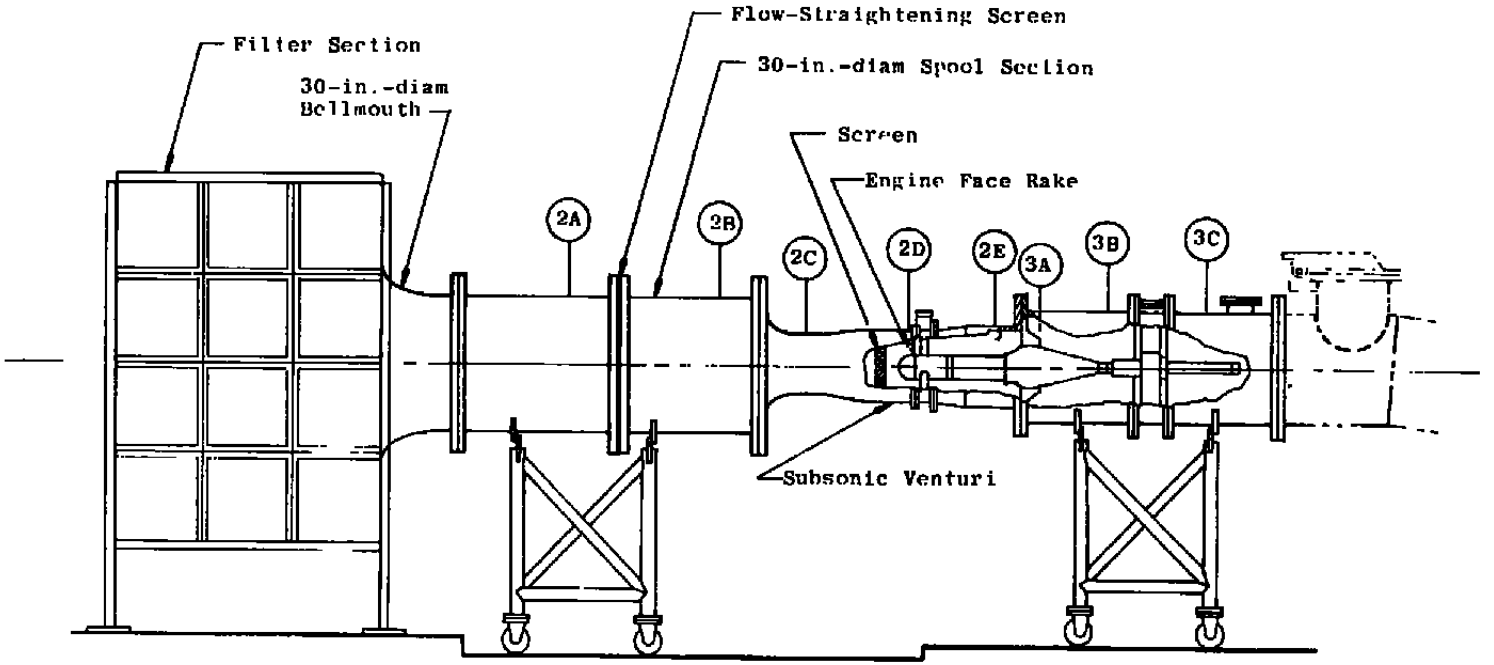

Measurements	Station Identification							
	2A	2B	2C	2D	2E	3A	3B	3C
Total Pressure				16	5			
Static Pressure (Wall)	2	8	8	2		2	4	2
Total Temperature		6			5			
Skin Temperature			2			4		

Figure 10. Test installation — atmospheric inbleed.

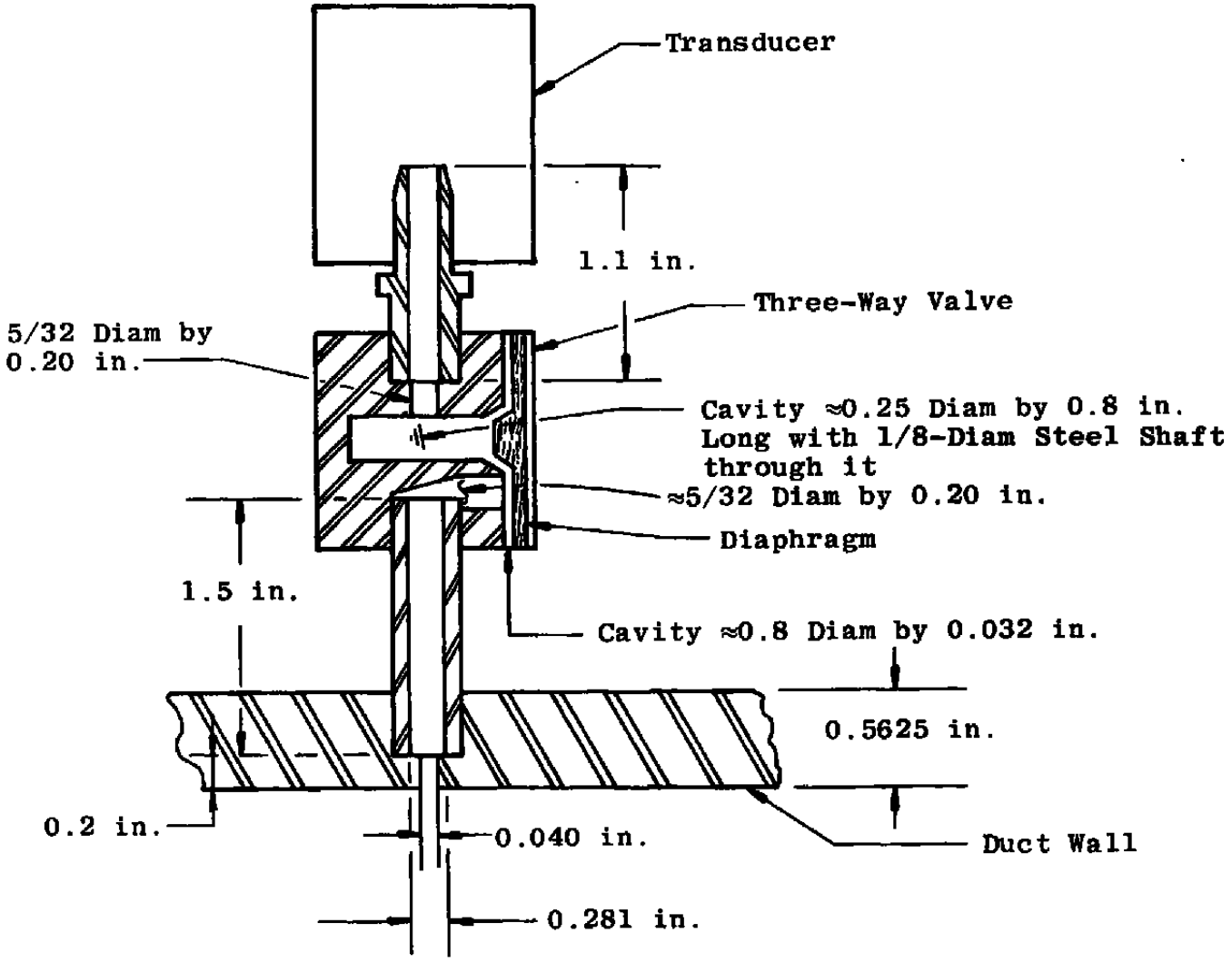

Figure 11. Close-coupled absolute pressure transducer installation.

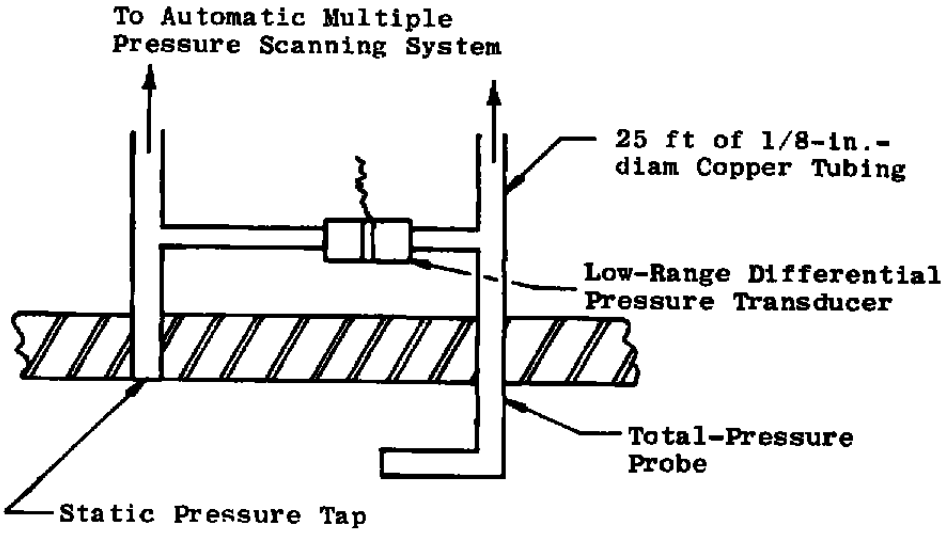

a. Differential pressure mode

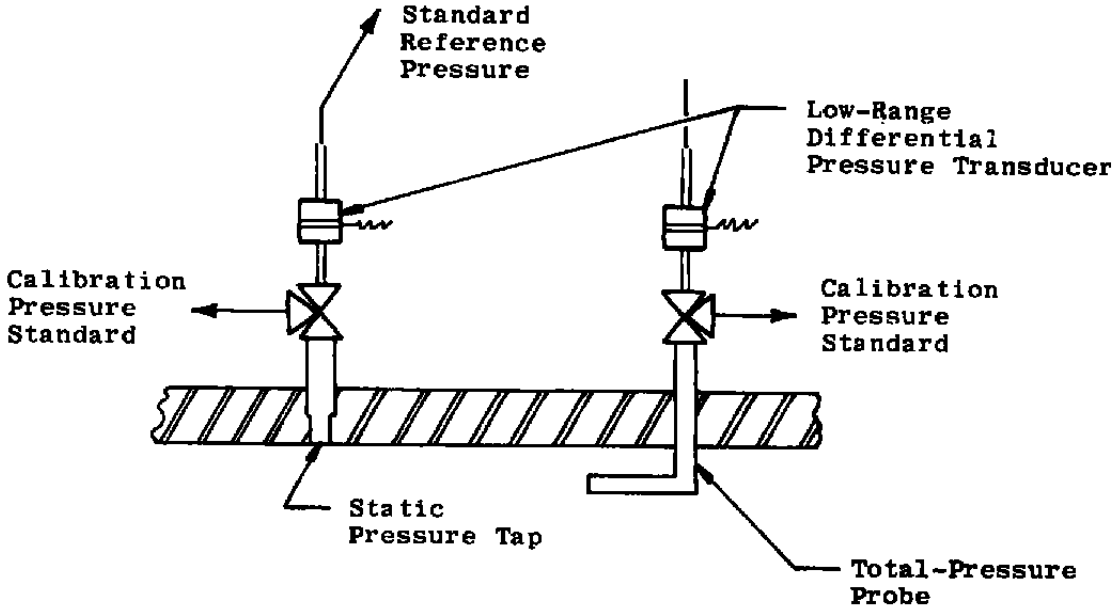

b. Absolute pressure mode

Figure 12. Bellmouth differential pressure transducer systems.

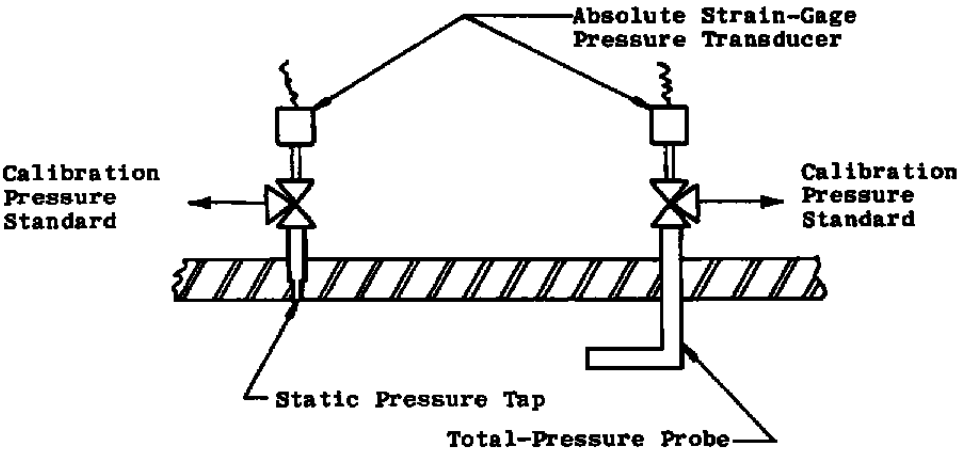

Figure 13. Close-coupled absolute pressure system.

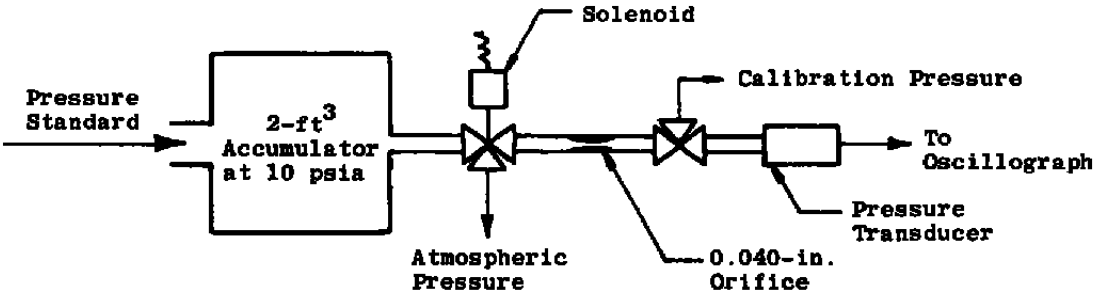

Figure 14. Pressure pulse generator.

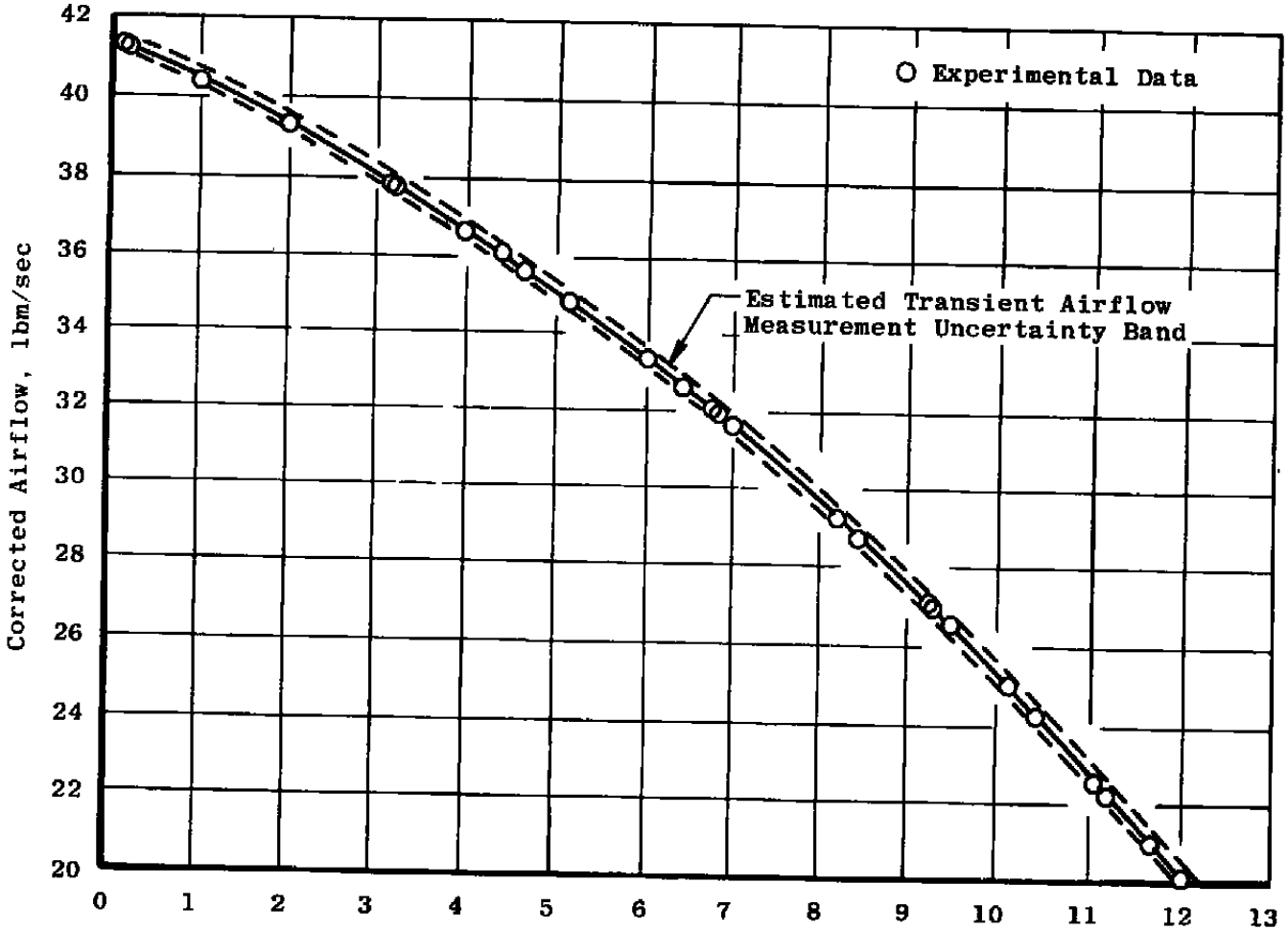

a. Shroud Configuration A

Figure 15. Turbine engine transient airflow simulator calibration curve.

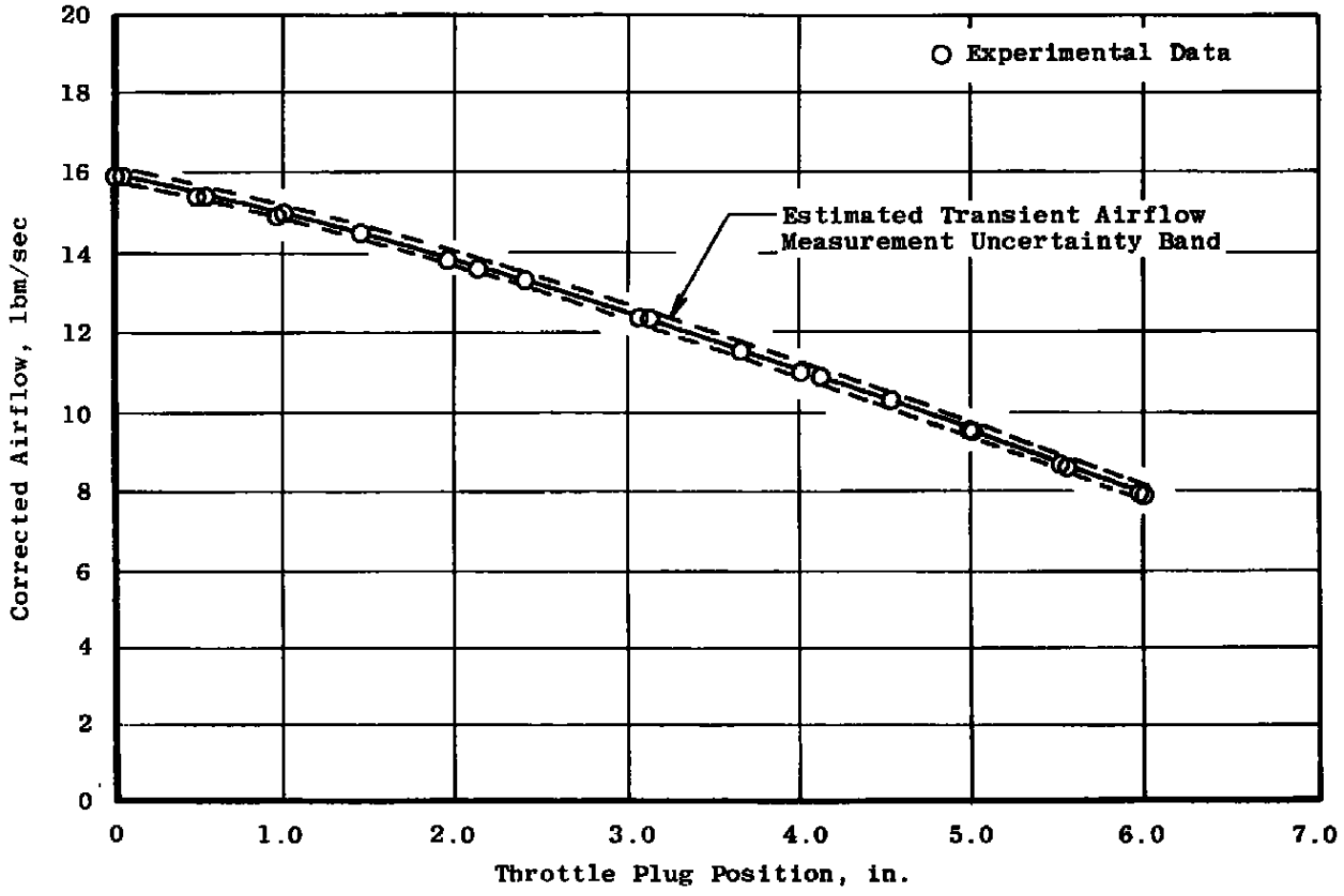

b. Shroud Configuration B
Figure 15. Concluded.

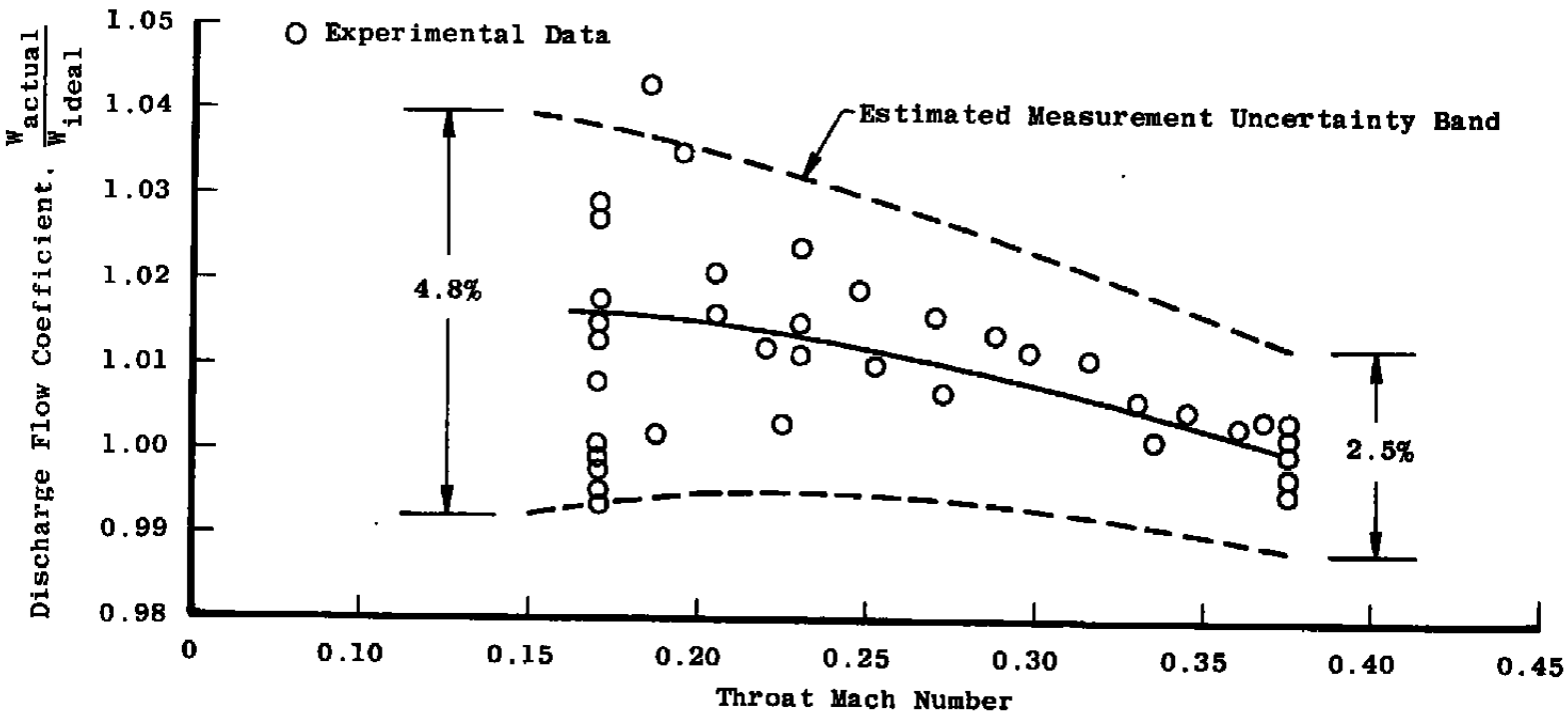

Figure 16. Bellmouth calibrated flow coefficient using piezoresistive pressure transducers in the differential mode.

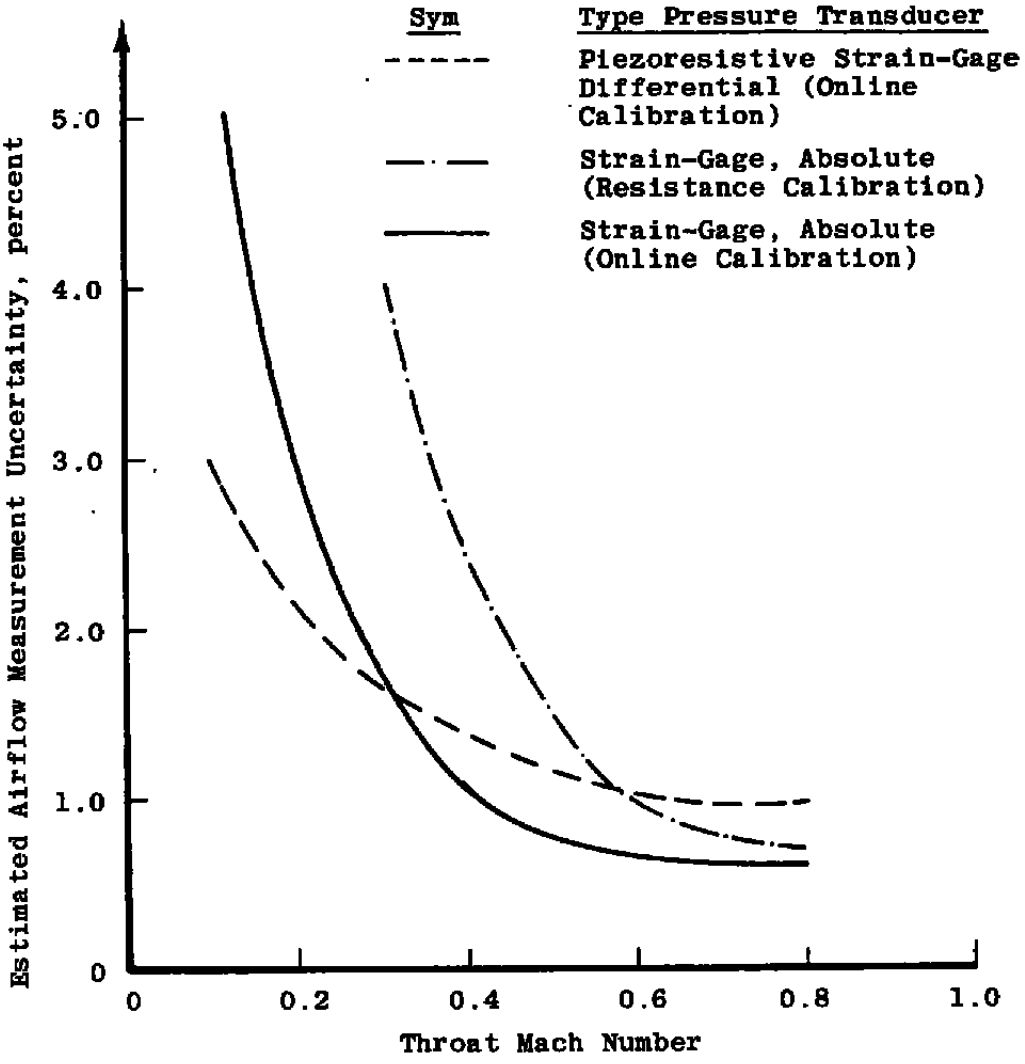

Figure 17. Engine bellmouth transient airflow estimated measurement uncertainty using different pressure transducers and calibration systems.

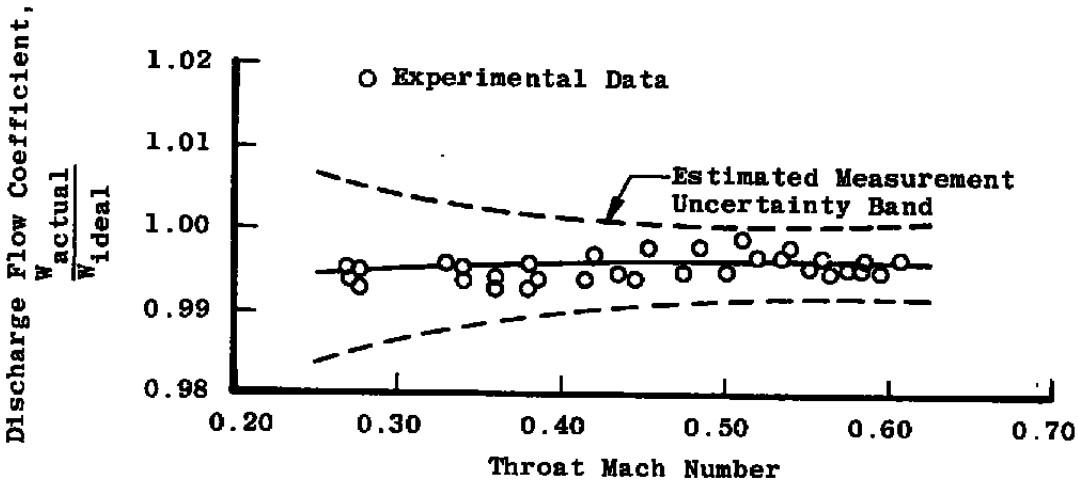

Figure 18. Subsonic venturi calibrated flow coefficient.

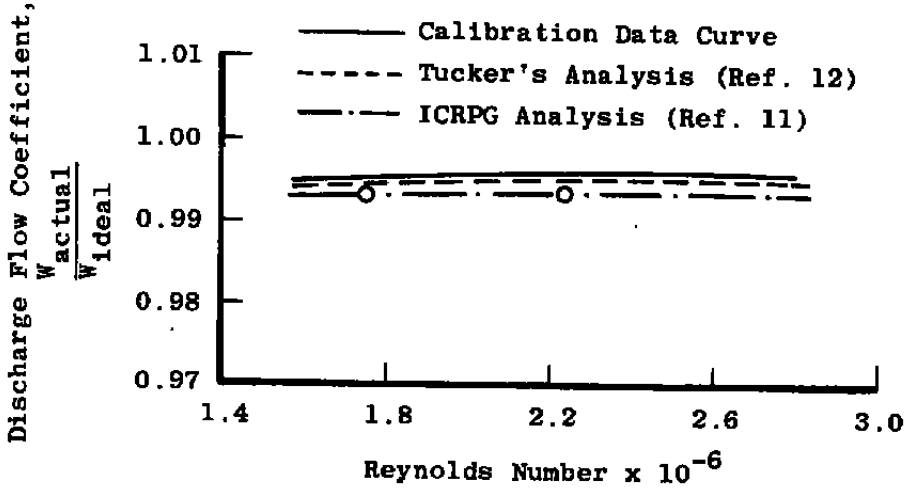

Figure 19. Subsonic venturi experimental/theoretical flow coefficient comparison.

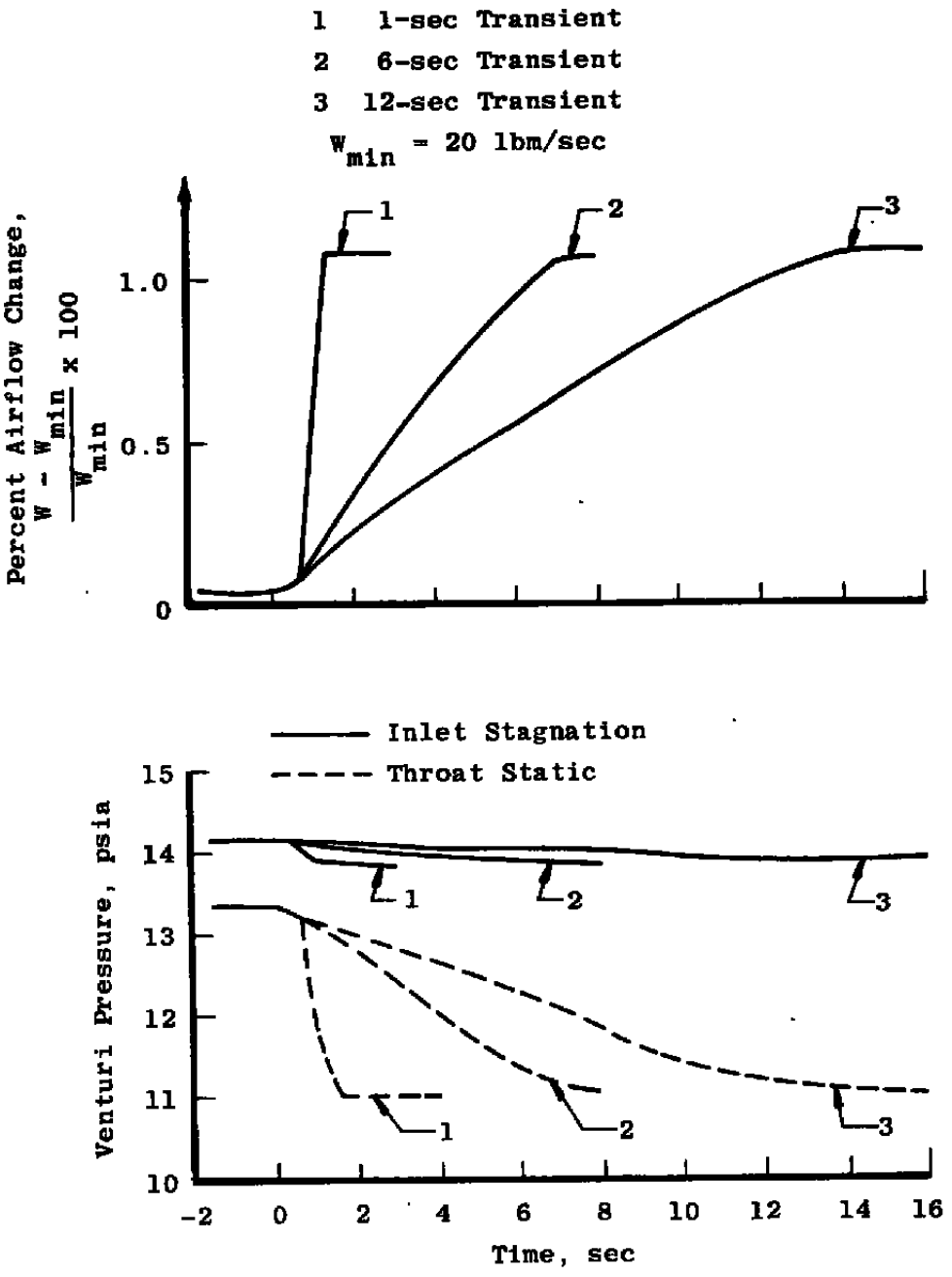

a. Transient flow conditions

Figure 20. Subsonic venturi transient performance (acceleration).

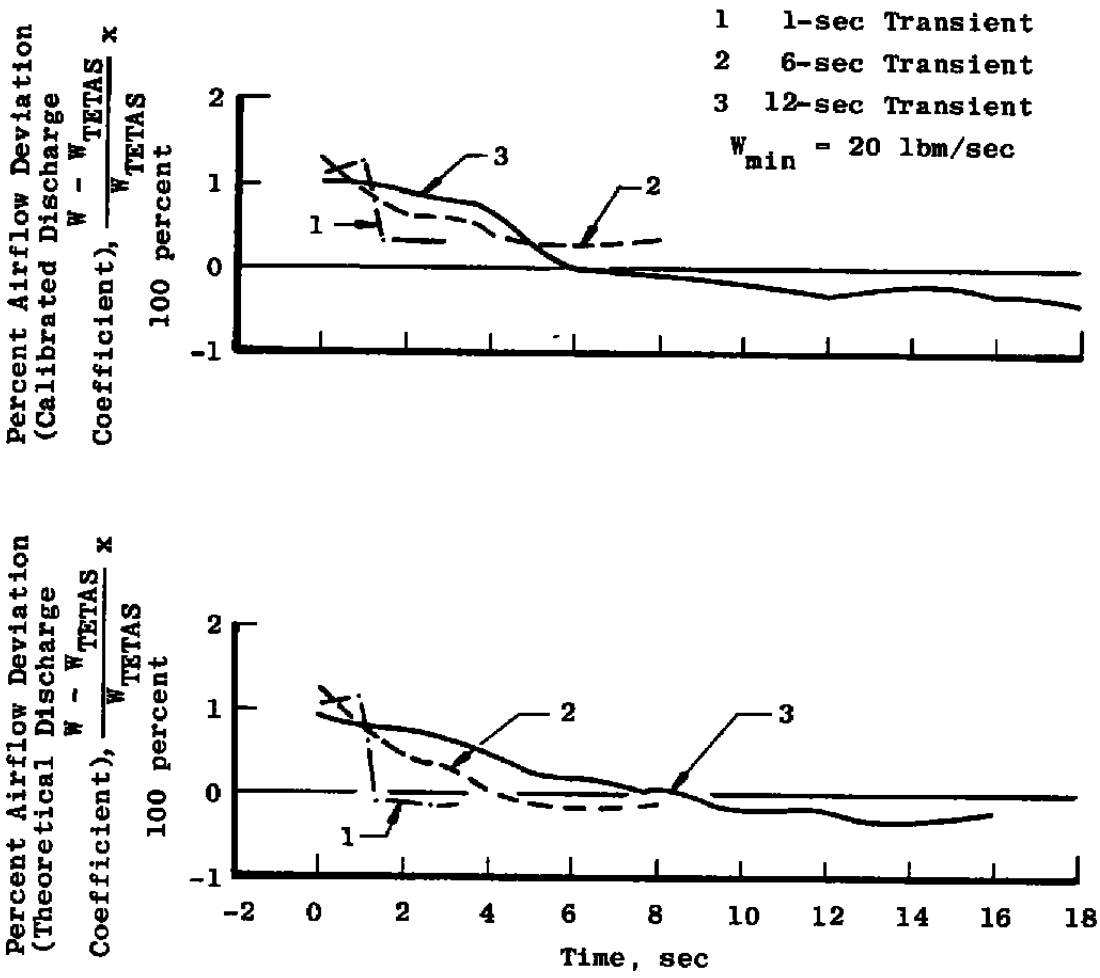

b. Deviation from TETAS airflow
Figure 20. Concluded.

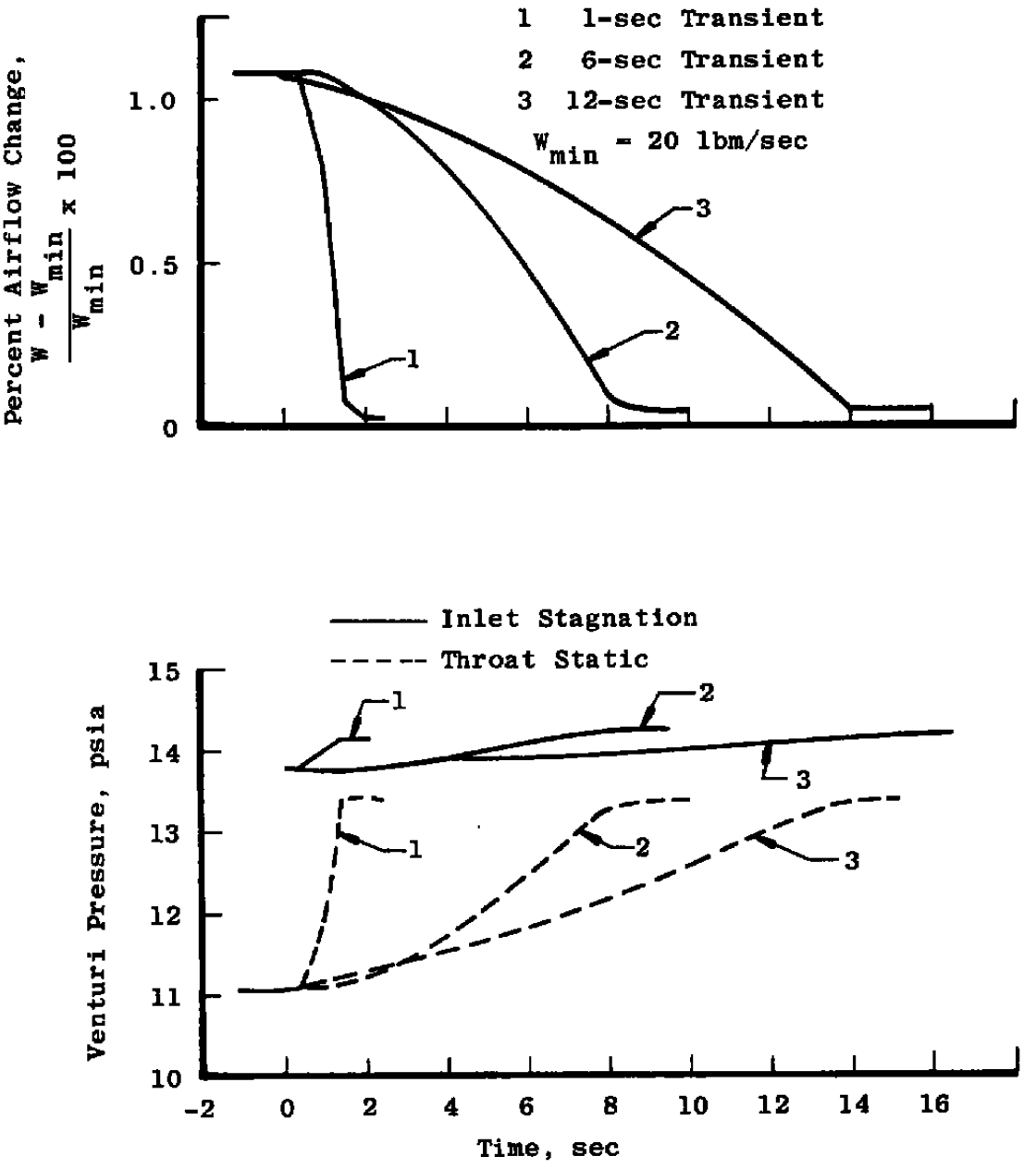

a. Transient flow conditions

Figure 21. Subsonic venturi transient performance (deceleration).

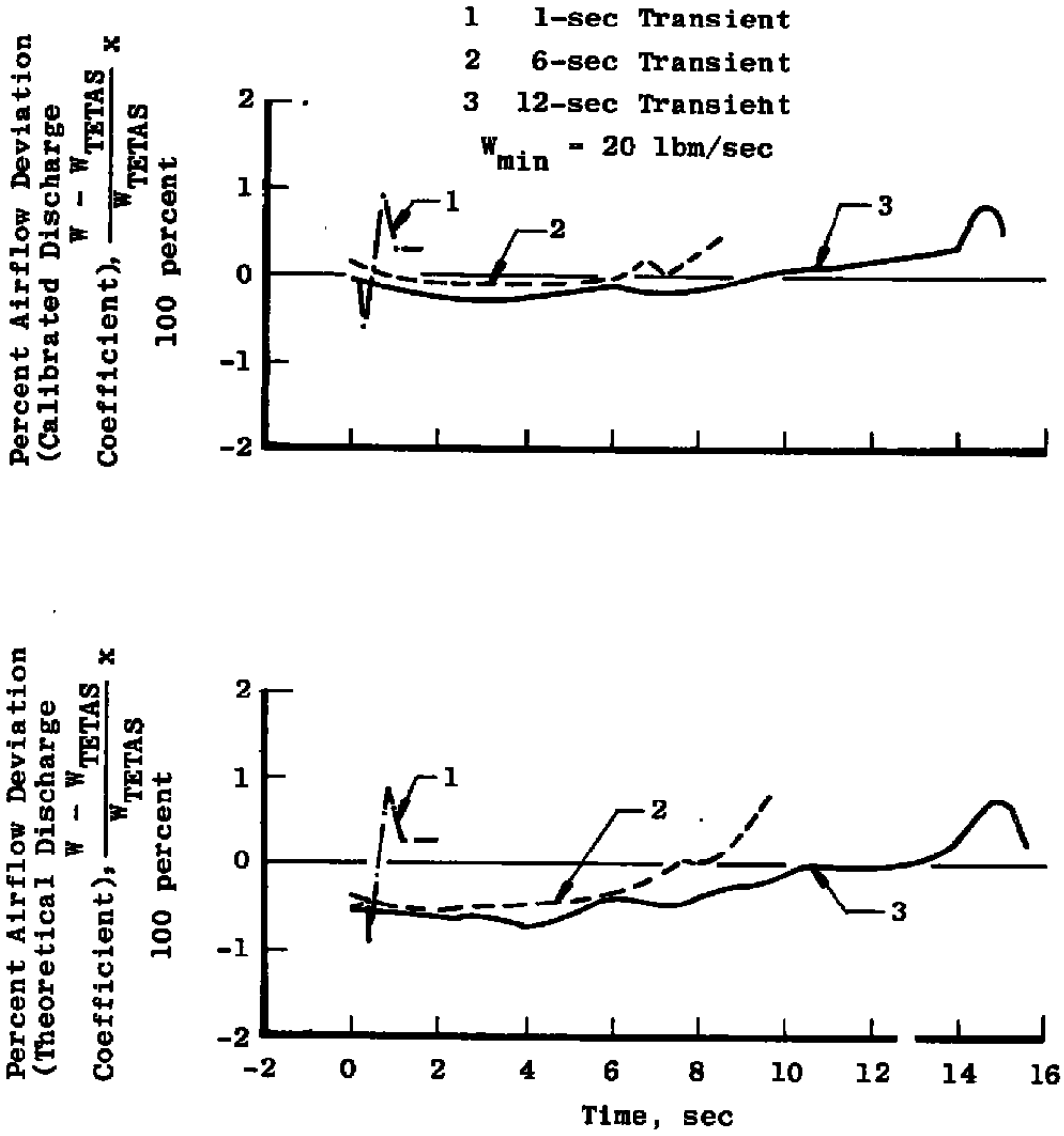

b. Deviation from TETAS airflow
Figure 21. Concluded.

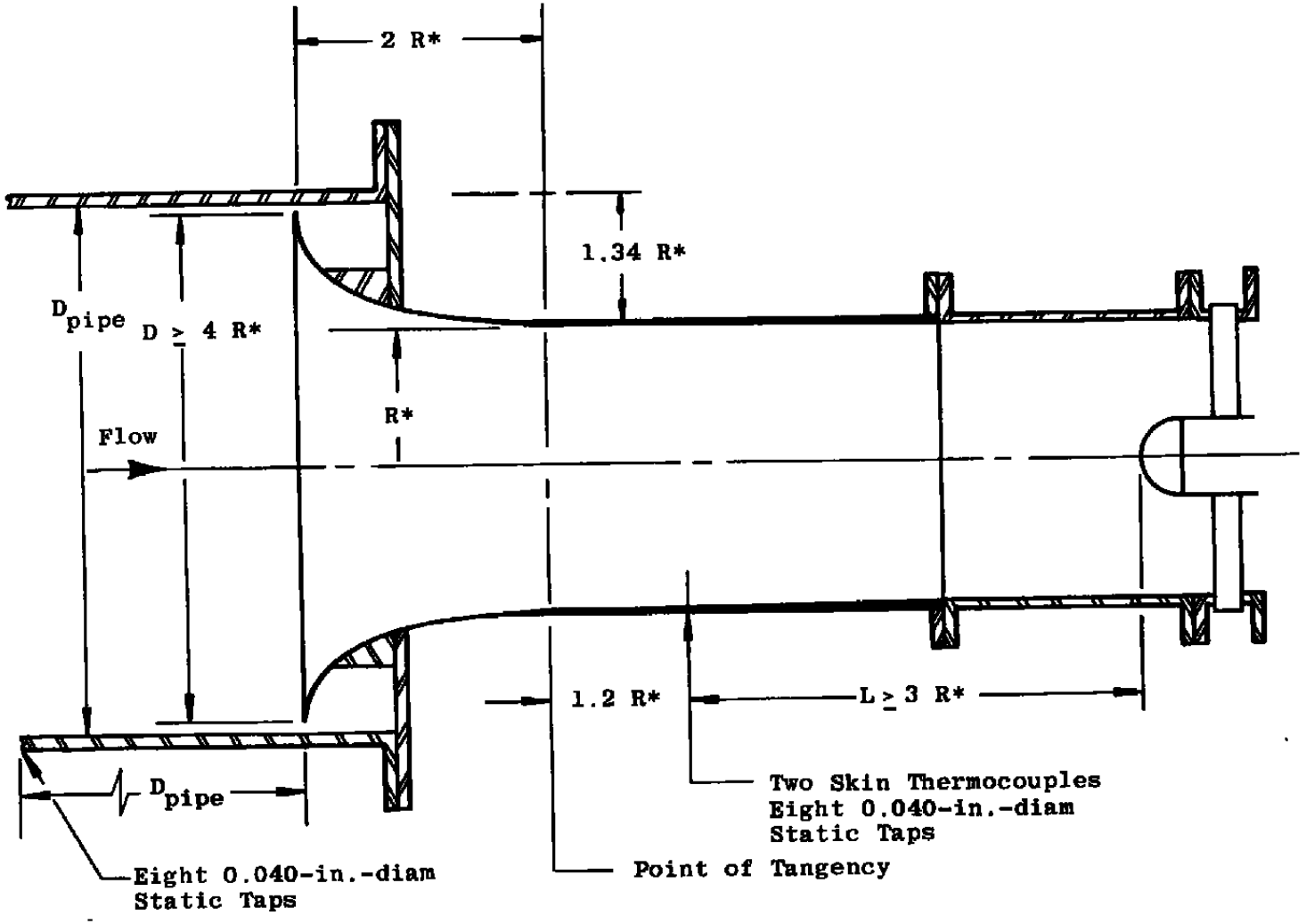

Figure 22. Recommended engine bellmouth design.

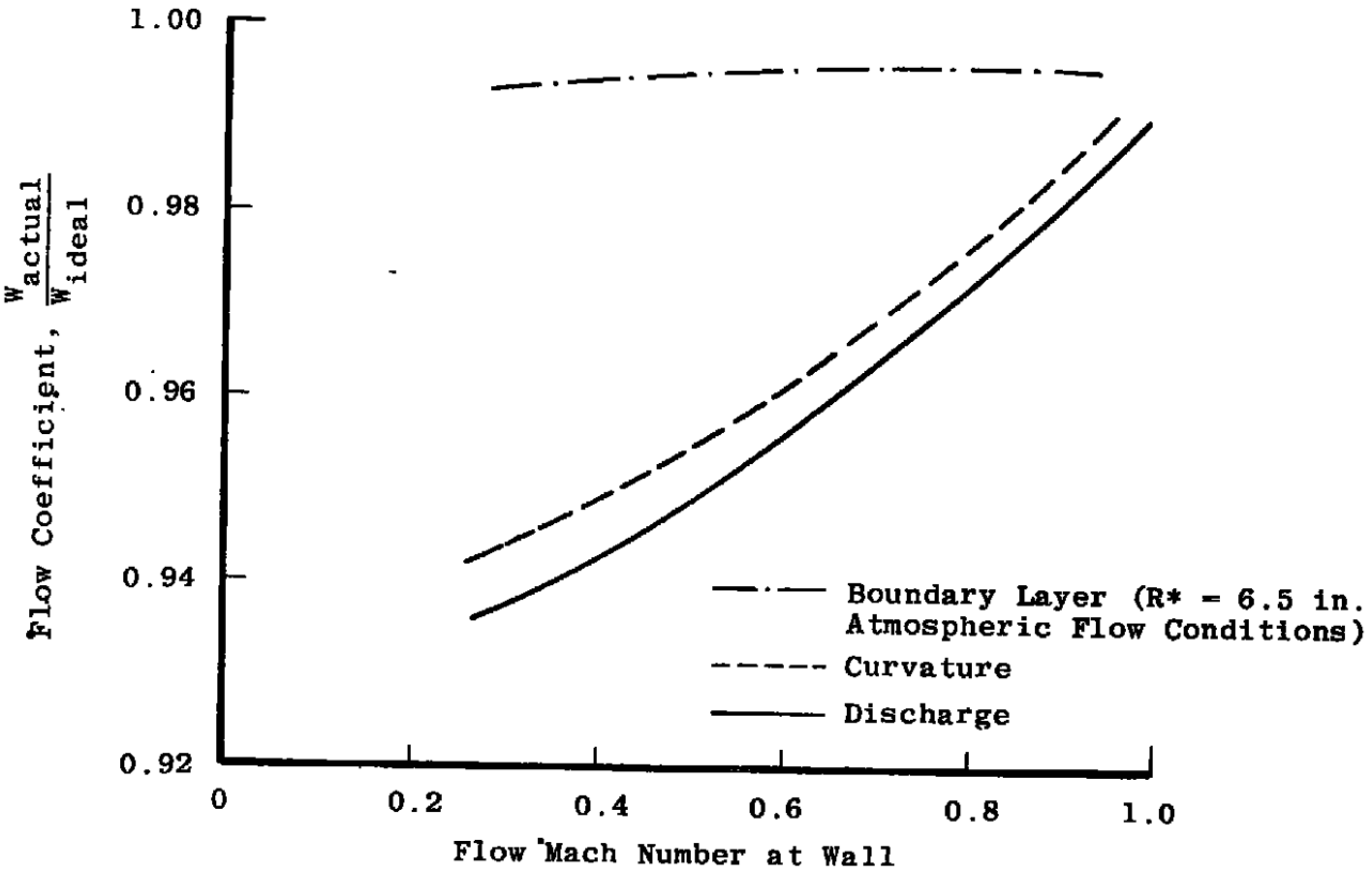

Figure 23. Sonic venturi flow coefficients.

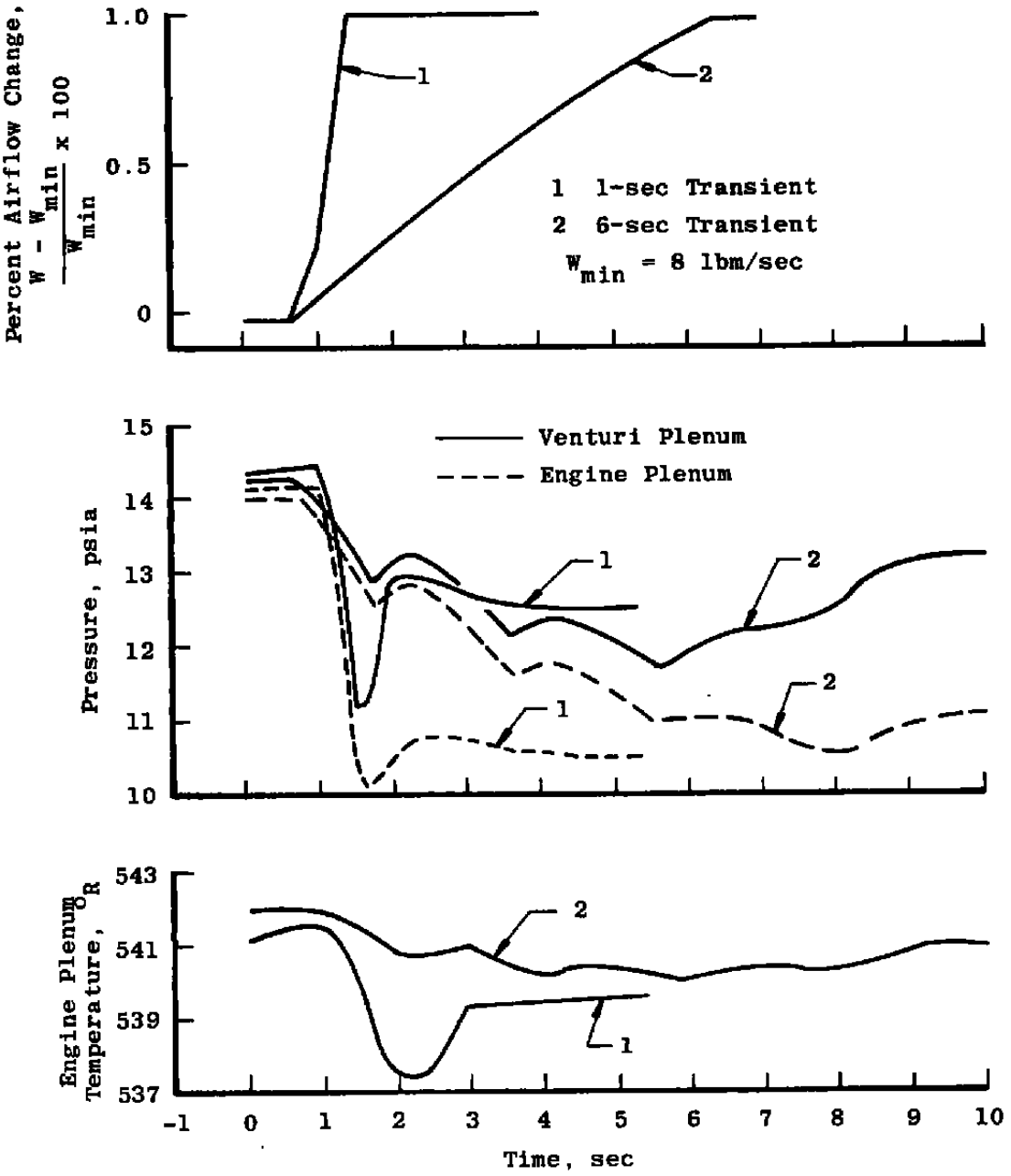

a. Transient flow conditions

Figure 24. Sonic venturi transient performance (acceleration).

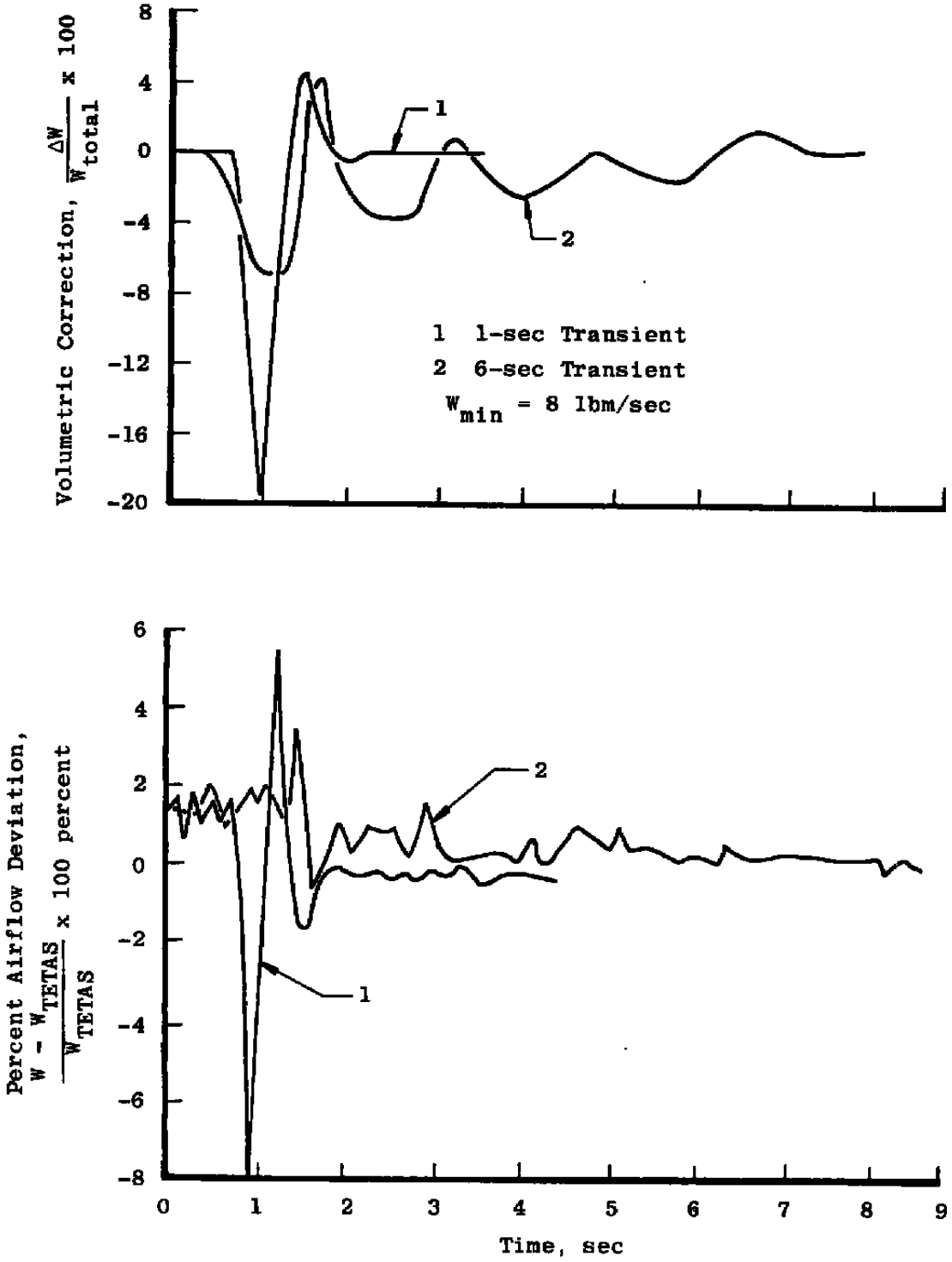

b. Deviation from TETAS airflow
Figure 24. Concluded.

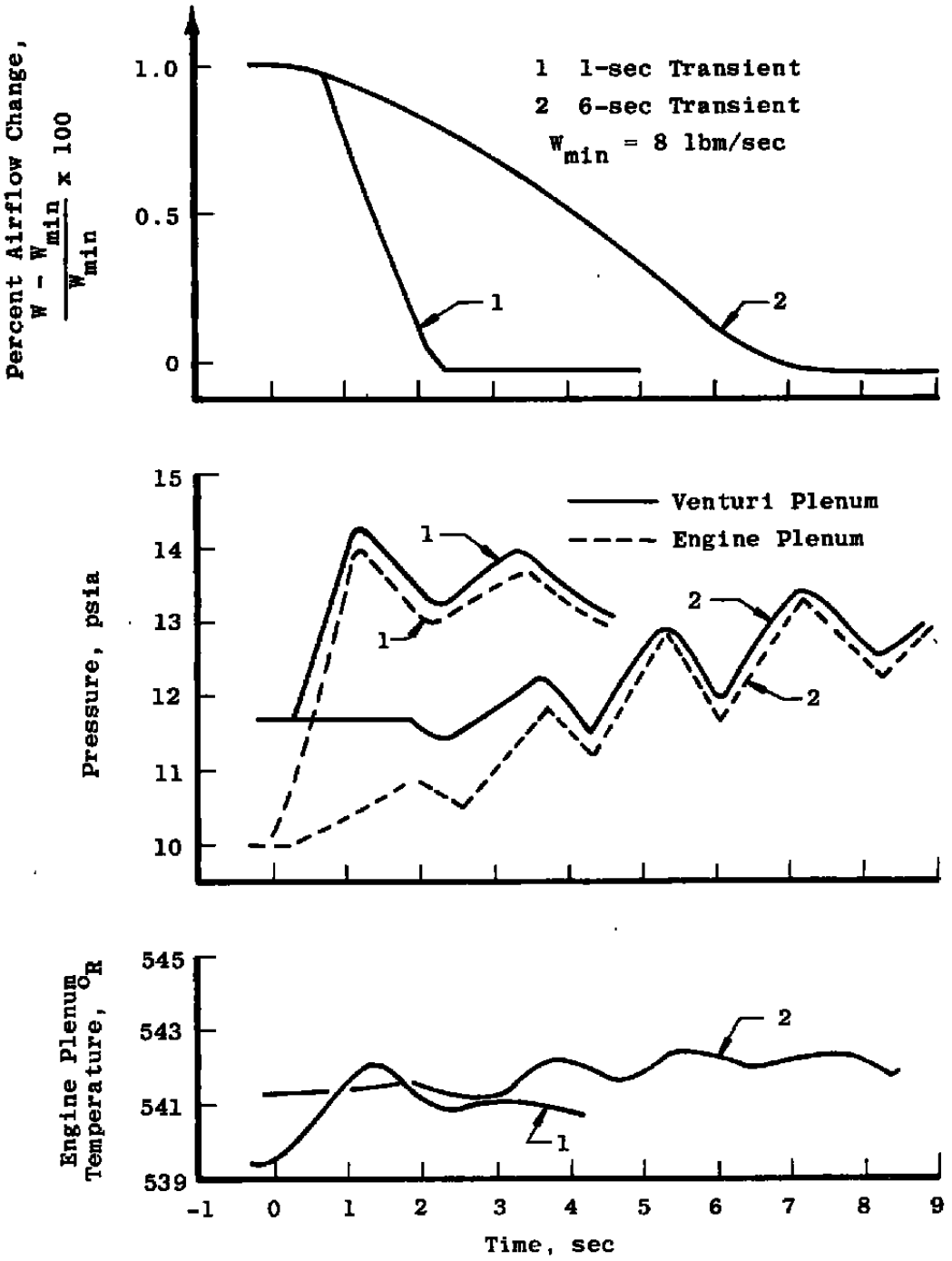

a. Transient flow conditions

Figure 25. Sonic venturi transient performance (deceleration).

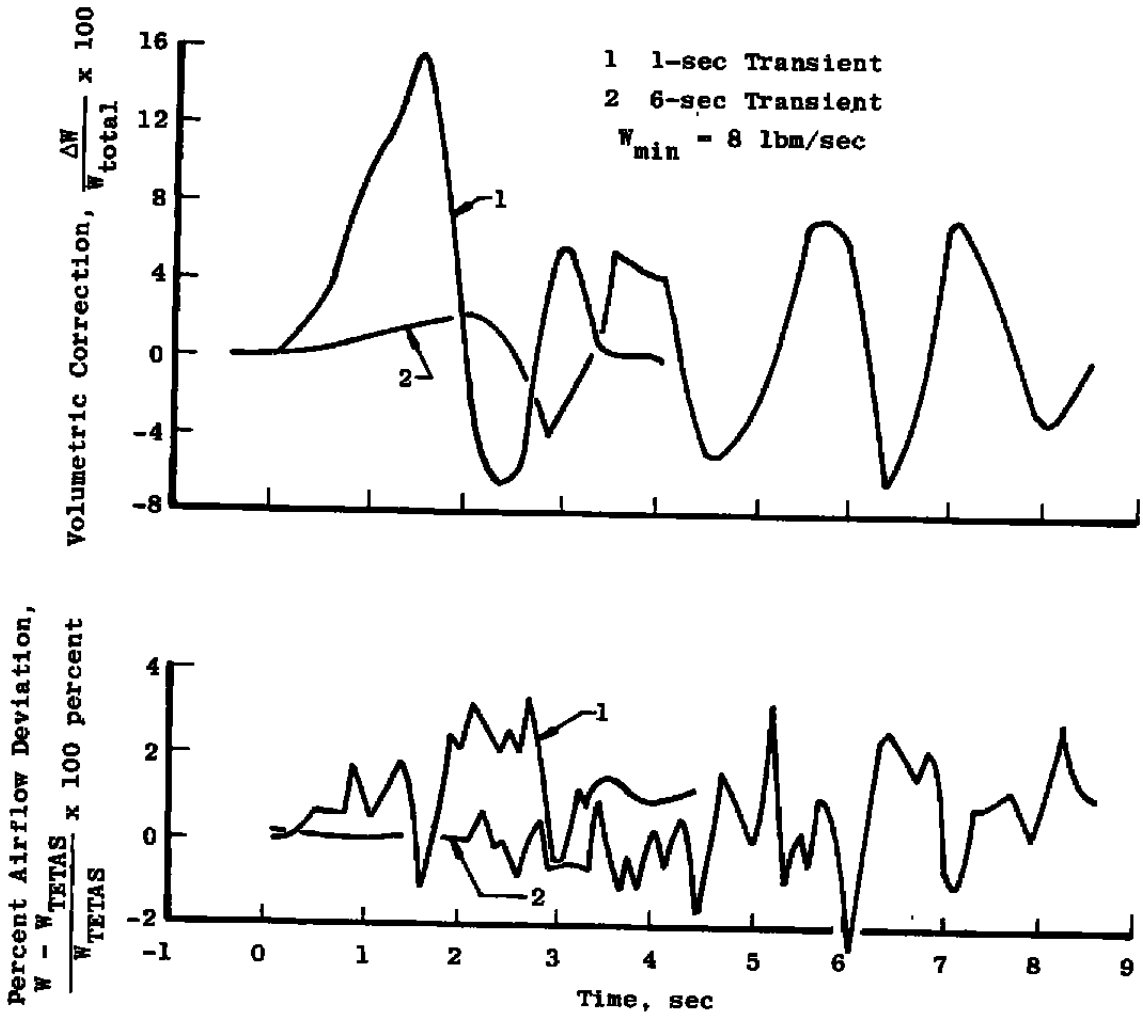

b. Deviation from TETAS airflow

Figure 25. Concluded.

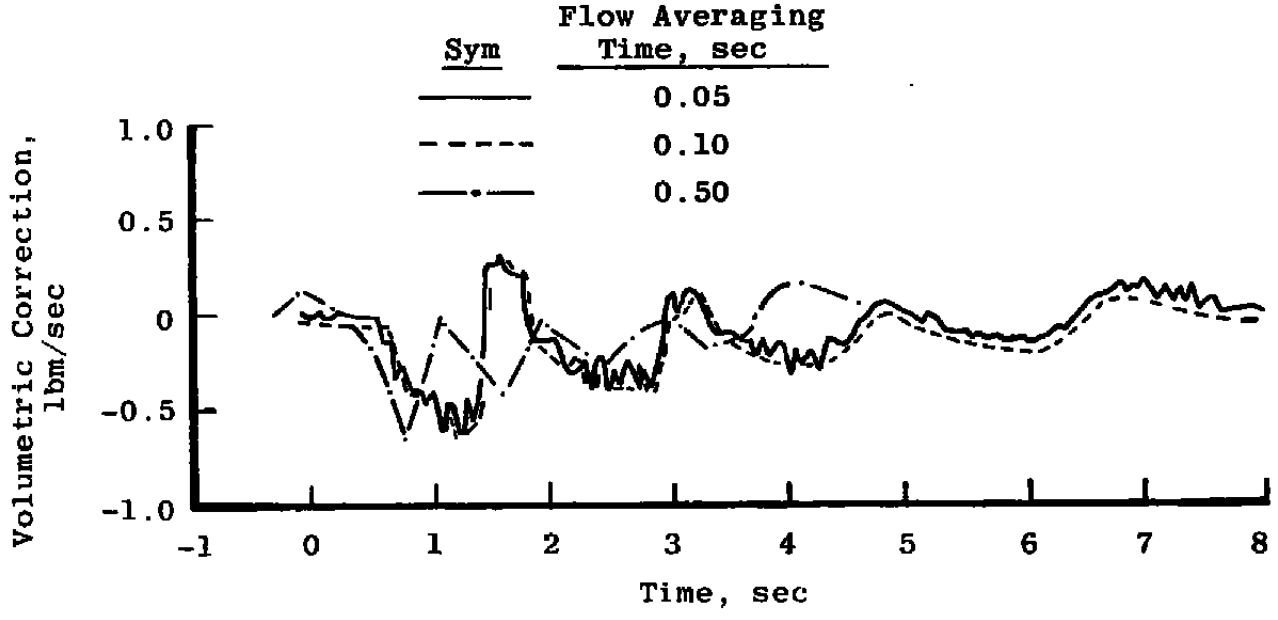

Figure 26. Effect of time average on volumetric mass flow correction.

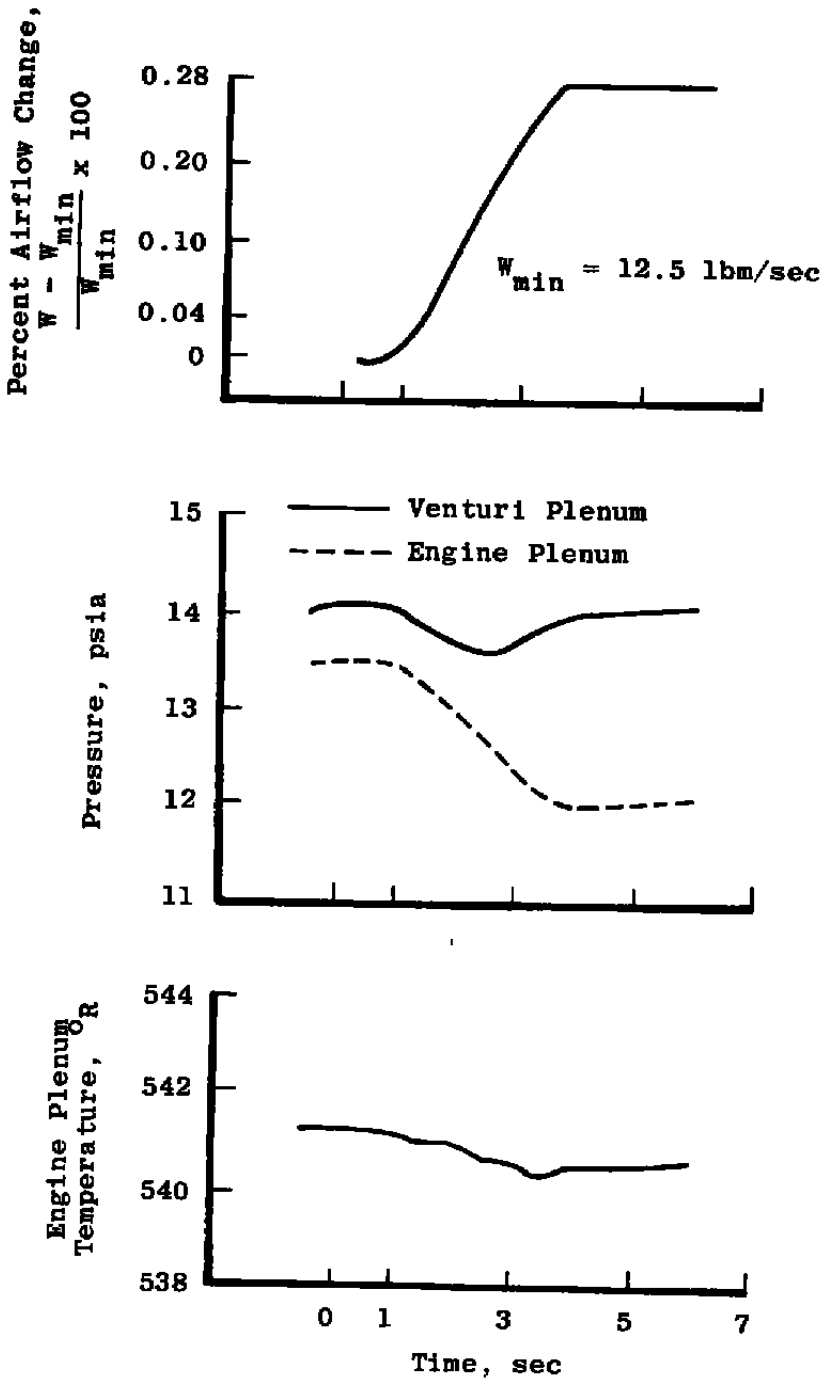

a. Transient flow conditions

Figure 27. Sonic venturi transient performance (partial deceleration).

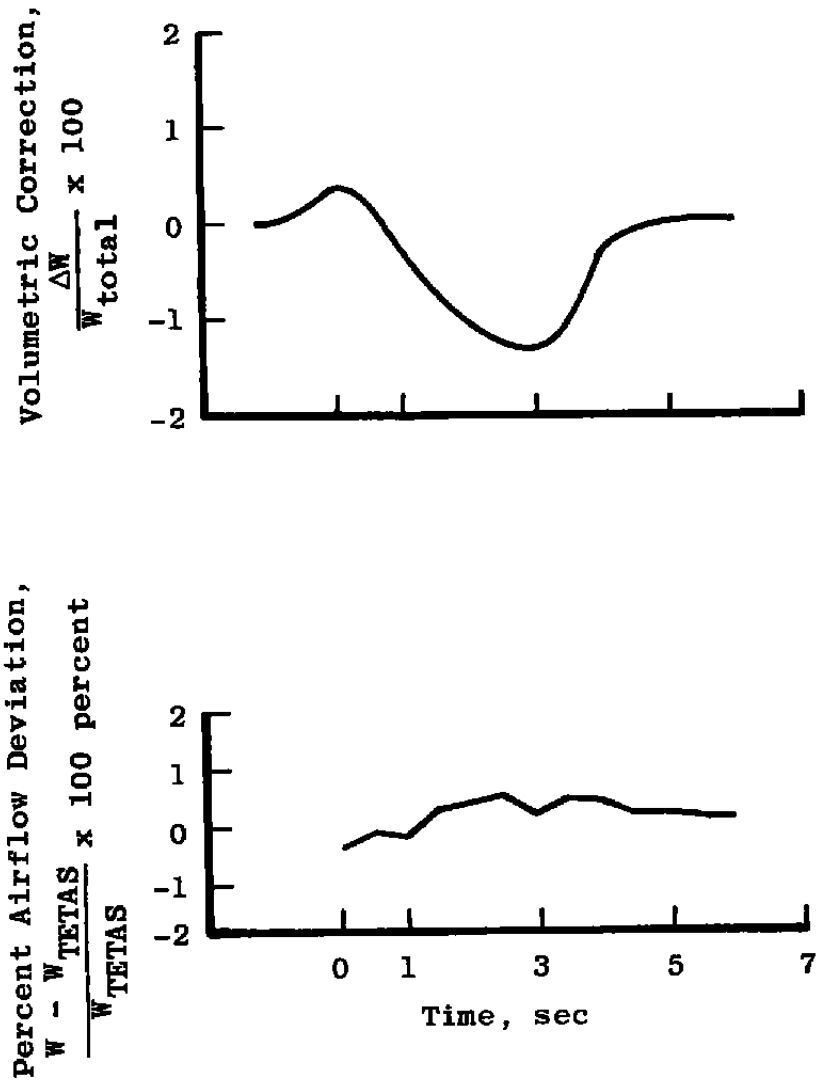

b. Deviation from TETAS airflow

Figure 27. Concluded.

Table 1. Parameter Measurement Uncertainties
a. Steady-State

Parameter Designation	STEADY-STATE ESTIMATED MEASUREMENT*							Range	Type of Measuring Device	Type of Recording Device	Method of System Calibration
	Precision Index (S)			Bias (B)		Uncertainty ±(B + tgsS)					
	Percent of Reading	Unit of Measurement	Degree of Freedom	Percent of Reading	Unit of Measurement	Percent of Reading	Unit of Measurement				
T2E	—	±0.6°F	31	—	±0.9°F	—	±2°F	20 to 100°F	Copper-Constantan Temperature Transducers	Sequential Sampling, Millivolt-to-Digital Converter, and Magnetic Tape Storage Data Acquisition System	Millivolt Substitution Based on the NBS Thermocouple Polynomials
T1C	—	±0.6°F	31	—	±0.9°F	—	±2°F	20 to 100°F	Chromel®-Alumel® Temperature Transducers		
TTI	—	±0.6°F	31	—	±0.9°F	—	±2°F	20 to 100°F			
PS1D (1-6)	±0.09	—	31	±0.07	—	±0.25	—	10 to 50 psia	Bonded Strain-Gage-Type Pressure Transducers	Automatic Multiple Pressure Scanning System onto Sequential Sampling, Millivolt-to-Digital Converter, and Magnetic Tape Storage Data Acquisition System	Resistance Shunt Based on the Standards Laboratory Determination of Transducer Applied Pressure versus Resistance Shunt Equivalent Pressure Relationship
PS1D (Average)	±0.04	—	31	±0.07	—	±0.15	—				
PS1D (1-4)	±0.09	—	31	±0.07	—	±0.25	—	10 to 15 psia		Sequential Sampling, Millivolt-to-Digital Converter, and Magnetic Tape Storage Data Acquisition System	In-Place Application of Multiple Pressure Levels Measured with a Pressure-Measuring Device Calibrated in the Standards Laboratory
PS1E (Average)	±0.05	—	31	±0.07	—	±0.17	—				
P2E (1-5)	±0.09	—	31	±0.07	—	±0.25	—	10 to 15 psia			
P2E (Average)	±0.04	—	31	±0.07	—	±0.15	—				
PS2B (2-8)	±0.09	—	31	±0.07	—	±0.25	—	10 to 15 psia			
PS2B (Average)	±0.03	—	31	±0.07	—	±0.13	—				
PS2C (1-7)	±0.09	—	31	±0.07	—	±0.25	—	10 to 15 psia			
PS2C (Average)	±0.03	—	31	±0.07	—	±0.13	—				
POS	—	±0.02 in.	31	—	±0.02 in.	—	±0.06 in.	0 to 12 in.	Encoder		In-Place Measurement of Physical Dimensions versus Transducer Output

Table 1. Concluded
b. Transient

Parameter Designation	ESTIMATED MEASUREMENT*							Range		Type of Measuring Device	Type of Recording Device	Method of System Calibration
	Precision Index (S)			Bias (B)		Uncertainty ±(B + t_{95}S)						
	Percent of Reading	Unit of Measurement	Degree of Freedom	Percent of Reading	Unit of Measurement	Percent of Reading	Unit of Measurement	Amplitude	Frequency			
T2E	—	±0.7°F	31	—	±2.6°F	—	±4°F	20 to 100°F	0.1 Hz	Chromel®-Alumel® Temperature Transducers	Sequential Sampling, Millivolt-to-Digital Converter, and Magnetic Tape Storage Data Acquisition System	Millivolt Substitution Based on the NBS Thermocouple Polynomials
T1C	—	±0.7°F	31	—	±2.6°F	—	±4°F	20 to 100°F	0.1 Hz			
TT1	—	±0.7°F	31	—	±2.6°F	—	±4°F	20 to 100°F	0.1 Hz			
PS1D (1-6)	±0.15	—	31	±0.1	—	±0.4	—	10 to 50 psia	3 Hz	Bonded Strain-Gage-Type Pressure Transducers	Automatic Multiple Pressure Scanning System onto Sequential Sampling, Millivolt-to-Digital Converter, and Magnetic Tape Storage Data Acquisition System	Resistance Shunt Based on the Standards Laboratory Determination of Transducer Applied Pressure versus Resistance Shunt Equivalent Pressure Relationship
PS1D (Average)	±0.06	—	31	±0.1	—	±0.22	—					
PS1E (1-4)	±0.15	—	31	±0.1	—	±0.4	—	10 to 15 psia	3 Hz		Sequential Sampling, Millivolt-to-Digital Converter, and Magnetic Tape Storage Data Acquisition System	In-Place Application of Multiple Pressure Level Measured with a Pressure-Measuring Device Calibrated in the Standards Laboratory
PS1E (Average)	±0.08	—	31	±0.1	—	±0.26	—					
PS2E (1-5)	±0.15	—	31	±0.1	—	±0.4	—	10 to 15 psia	3 Hz			
PS2E (Average)	±0.07	—	31	±0.1	—	±0.24	—					
PS2B (2-8)	±0.15	—	31	±0.1	—	±0.4	—					
PS2B (Average)	±0.06	—	31	±0.1	—	±0.22	—					
PS2C (1-7)	±0.15	—	31	±0.1	—	±0.4	—					
PS2C (Average)	±0.06	—	31	±0.1	—	±0.22	—					

Table 2. Steady-State Sonic Venturi Critical Flow Uncertainty

Parameter Designation	Precision Index, Percent of Reading	Bias, Percent of Reading	Influence Coefficient on Airflow
PSID (Average)	±0.04	±0.07	1.0
T1C	±0.115 at 520°R	±0.173 at 520°R	0.5
Throat Area	---	±0.1	1.0
Flow Coefficient	---	±0.20	1.0
Airflow	±0.07	±0.25	---

±Airflow Uncertainty = ± (Bias + t_{95} Precision) = 0.39 percent

Table 3. Turbine Engine Transient Airflow Simulator Measurement Uncertainty

Parameter Designation	Precision Index, Percent of Reading	Bias, Percent of Reading	Influence Coefficient on Airflow
$W_{venturi}$	±0.07	±0.25	1.0
P2E, Avg.	±0.04	±0.07	1.0
T2E	±0.115 at 520°R	±0.173 at 520°R	0.5
WAC	±0.1	±0.27	1.0
POS			
at 12 in.	±0.17	±0.17	1.7*
at 6 in.	±0.33	±0.33	1.4**
at 0 in.	---	---	0†
TETAS Airflow			
at 12 in.	±0.31*	±0.46*	---
at 6 in.	±0.47**	±0.55**	---
at 0 in.	±0.1†	±0.27†	---

±Transient Airflow Uncertainty = ± (Bias + t_{95}) Precision

U at 12 in. = 1.0 percent (Min. Flow)

U at 6 in. = 1.5 percent (Min. Flow)

U at 0 in. = 0.5 percent (Max. Flow)

*Shroud Configuration A

**Shroud Configuration B

†Shroud Configurations A and B

APPENDIX A
SUBSONIC VENTURI SIZING PROCEDURE

In order to size the subsonic venturi throat diameter, an estimate of the pressure drop across the exit-flow-straightener screens is required. The subsonic venturi used in this study was sized on the basis of Screen Configuration A (Fig. 7a) and the pressure loss curves defined in Ref. 16. The curves in Ref. 16 are for a single uniform screen; therefore, the first task is to define an equivalent single stream flow area factor for Screen Configuration A. Screen Configuration A is composed of

1. a 16-in. diameter, basic safety-support grid with 90-percent open area,
2. a 16-in. diameter, 4- by 4-in. mesh screen with 76-percent open area, and
3. a 13.7-in.-diameter, overlay 6- by 6-in. mesh screen with 66-percent open area.

Therefore, for 73 percent of the duct cross-sectional area [i.e., $(13.7/16)^2 \times 100$], the flow area is

$$(1 - \beta)_{inner} = (0.9 \times 0.76 \times 0.66) \times 100 = 45 \text{ percent}$$

For the outer 27 percent of the duct area (i.e., 1 -0.73), the flow area is

$$(1 - \beta)_{outer} = (0.9 \times 0.76) = 68 \text{ percent}$$

The effective single screen total flow area is

$$(1 - \beta)_{eff} = (0.73 \times 45) + (0.27 \times 68) = 52 \text{ percent}$$

The subsonic venturi inlet flow stagnation conditions are (1) P = 14 psia and (2) T = 520°R, and the screen approach flow area is 202 in.^{2} By using this information and the pressure loss curves for a 52-percent flow area (Ref. 16), a mass-flow pressure-loss curve can be generated for Screen Configuration A (Fig. A-1). By using the simulator or engine maximum airflow rating which, for the present case, is a corrected airflow of 42 lbm/sec, the following expression can be written:

$$WAC_{max} = 42 \times \left(\frac{\sqrt{520}}{14.966} \right)_{atmospheric} \times \left(\frac{P\left(1 - \frac{\Delta P}{P}\right)}{\sqrt{T}} \right)_{actual}$$

which for the present stagnation flow conditions reduces to

$$WAC_{max} = 40.01 (1 - \Delta P/P)$$

This equation is also plotted in Fig. A-1. The point at which the two curves cross indicates the estimated maximum airflow achievable with the calculated screen blockage. For the present case, the estimated maximum airflow is 36 lbm/sec. The subsonic venturi was sized to have a maximum throat Mach number of 0.65, which is a compromise value based on measurement uncertainty requirements; allowance is made for some in-place flow-screen blockage adjustments that may be required. For a maximum airflow of 36 lbm/sec, P = 14 psia, T = 520°R, and throat flow Mach number of 0.65, the subsonic venturi throat diameter is 12.6 in. For this throat size, the estimated minimum flow throat Mach number for the engine simulation is 0.26.

The actual pressure drop for Configuration A is shown in Fig. A-2. The actual pressure drop exceeds the estimated value and corresponds to an effective single-screen total-flow area of approximately 48 percent, instead of 52 percent, which was estimated. The current estimating procedure for multiple-screen overlays, however, is considered adequate for sizing the venturi throat.

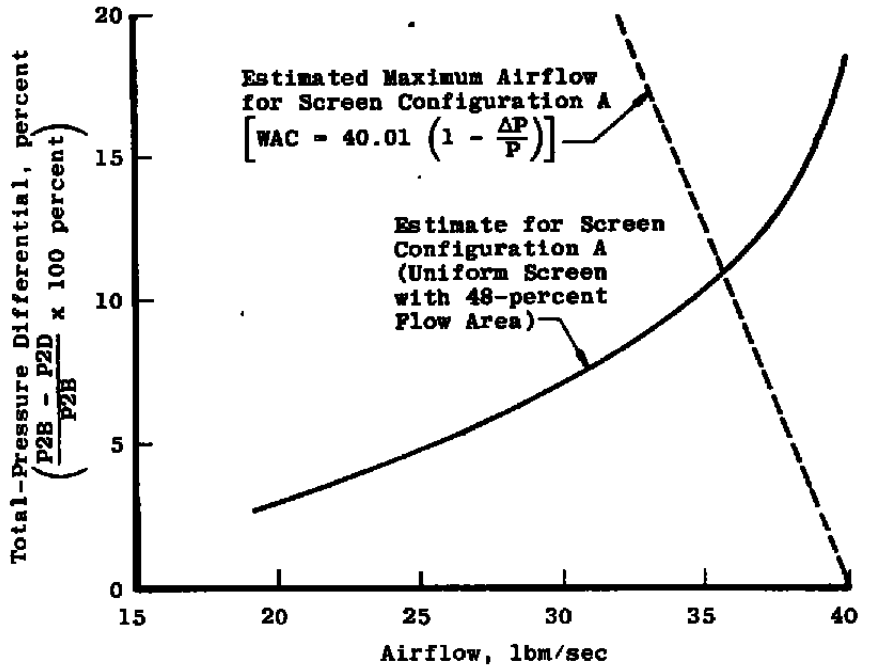

Figure A-1. Pressure loss curve for screen Configuration A.

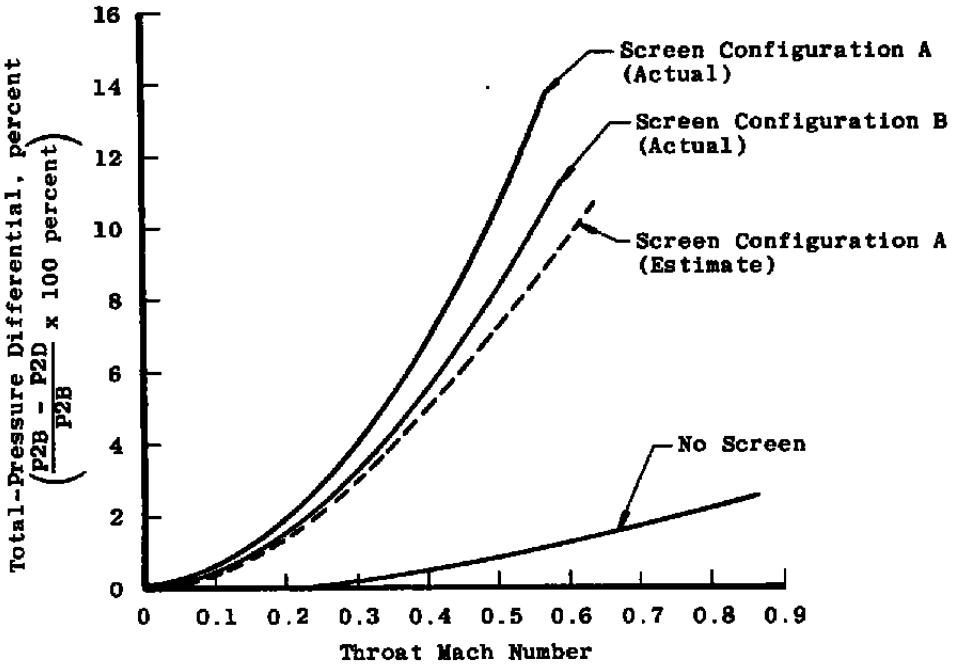

Figure A-2. Subsonic venturi pressure losses (98-percent flow area).

APPENDIX B
INLET FLOW-CONDITIONING REQUIREMENTS

Inlet airflow-conditioning requirements must relate to acceptable limits of spatial distortion in flow properties. Inlet flow-distortion requirements for stagnation pressure and temperature were estimated by using the analysis presented in Ref. 11. Calculations were made for a sonic venturi operating at both critical and subcritical throat flow conditions. The evaluation consisted of comparing flow fields with uniform and with radial variations of 5 percent in both stagnation pressure and temperature. The radial variations were parabolic, with the maximum value occurring on the nozzle centerline. For critical flow calculations in which and using area-weighted bulk flow values of stagnation pressure and temperature are used, there is less than 0.1 percent difference between the calculated mass flow rates for the distorted and uniform flow cases. The difference in airflow rates for subcritical flow is about 1 percent. Radial distortion has a greater effect on subcritical operation because of the additional error introduced by evaluating the throat wall Mach number. For a parabolic radial variation of 2 percent, the subcritical flow difference in calculated airflow rate is about 0.1 percent.

The inlet airflow-conditioning equipment used for the present study was adaptations of the equipment discussed in Ref. 14. A honeycomb composed of round tubes 1 in. in diameter and 6 in. long was used to remove nonaxial flow components. An inlet screen of 20-mesh wire supported by a safety-support grid was used to provide a uniform-velocity profile. For the present study, the radial distortion of inlet stagnation pressure and temperature outside of the wall boundary layer was less than 2 percent where

$$\text{Distortion} = \left(\frac{\text{Maximum} - \text{Minimum}}{\text{Area-Weighted Average Value}}\right) \times 100$$

Radial distortion in temperature must be measured to determine area-weighted bulk values. Bulk values of total pressure, however, can be inferred by measuring the inlet plenum wall static pressure and accounting for the flow dynamic head because at low Mach numbers (i.e., less than 0.2), the static pressure is basically a one-dimensional value that corresponds to the airflow rate at a bulk stagnation pressure.

APPENDIX C
EXIT FLOW-CONDITIONING REQUIREMENTS

Exit airflow-conditioning requirements must relate to acceptable limits of spatial distortion in flow properties at the engine face station. Accepted engine face airflow quality goals for engine testing are (outside of the boundary layer region)

$$\frac{P_{max} - P_{min}}{P_{avg}} \leq 2 \text{ percent}$$

$$\frac{T_{max} - T_{min}}{T_{avg}} \leq 1 \text{ percent}$$

$$\frac{P_{rms}}{P_{avg}} \leq 1 \text{ percent}$$

The type of airflow-conditioning equipment used to meet these goals depends somewhat on the type of airflow metering system. For an engine bellmouth system, exit airflow-conditioning equipment is generally not required. For a sonic venturi isolated from the engine inlet, a flat perforated plate (i.e., a corebreaker) is generally used to disperse the high-velocity core flow that exists in the divergent portion of the venturi, and a 6- to 20-mesh screen supported by a safety-support grid (Fig. 9) is used to obtain a uniform-velocity profile. Exit airflow-conditioning equipment requirements for direct-connect subsonic venturis, however, are not established and will have to be developed with operational experience. In this program, a brief study was conducted to show that acceptable subsonic venturi exit airflow-conditioning equipment could be developed.

The exit flow quality of the subsonic venturi was evaluated by using three test configurations: (1) no screen, (2) overlay screen configuration with a safety-support system (Fig. 7a), and (3) a uniform screen configuration with a honeycomb support system (Fig. 7b).

The engine face airflow quality measurement systems used for the present study are discussed in Section 2.3.3. Figure C-1 presents the engine face radial total-pressure profiles for the three subsonic venturi airflow quality test configurations. The total-pressure profile for the no-screen configuration (Fig. C-1a) has a significant pressure distortion that is attributable to the effect of the diffuser adverse-pressure gradient on the wall boundary layer. The shape of the no-screen pressure profile suggests the use of a non-uniform screen design with increased flow blockage for the central portion of the flow.

Screen Configuration A (Fig. 7a) was designed with a screen overlay that increases the flow blockage for 73 percent of the central flow area. The total-pressure profiles for this configuration are presented in Fig. C-1b. The central stream flow blockage for Screen A was too large, as shown by the fact that the total-pressure profile deficiency occurs for the center of the flow and not at the wall, as occurred for the no-screen configuration. Therefore, by systematically reducing the overlay screen blockage, a uniform pressure profile can be achieved. The velocity and turbulence profiles for Screen Configuration A are shown in Figs. C-2 and C-3. A major portion of the resulting turbulence, which appears in Fig. C-3, resulted from the safety grid which was shown in Fig. 7. The safety grid itself contributes a turbulence level in the range of from 4 to 8 percent as is shown by Fig. C-4. The honeycomb and screen flow conditioning unit, Screen Configuration B (Fig. 7b), was investigated as a means of further reducing turbulence. Configuration B reduced the nominal turbulence levels to 2 to 3 percent as shown in Fig. C-5. The boundary layer produced by Configuration B is approximately the same thickness as that shown for screen A. Figure C-6 shows this velocity profile for the Configuration B flow conditioning. The fact that the radial velocity profile for Configuration B is apparently more uniform than the total pressure indicates that the radial static pressure profile is not uniform. A further reduction in turbulence can be accomplished through redesigning the supporting safety grid structure, reducing the grid blockage area.

No effort was made to refine the screens both because the refinement process is test peculiar and because the primary intention was only to illustrate that such designs can work. As further evidence, Fig. C-7 presents data obtained in a previous engine test program (Ref. 17). A flow conditioner similar to Screen Configuration A was used for this installation and a design was experimentally derived that met both the engine face pressure distortion and pressure fluctuation requirements. The current studies were conducted for adiabatic flows so that no assessment of temperature distortion was made. Total-temperature distortions, however, are generally the result of uninsulated walls or unmixed test cell inlet flows and not a product of the airflow metering system and, therefore, require separate correction considerations.

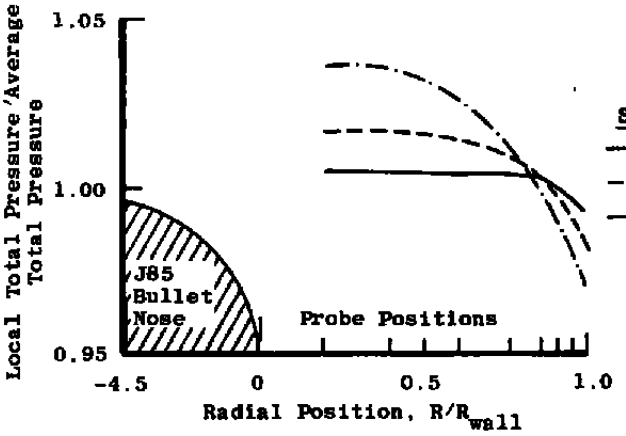

a. No screen

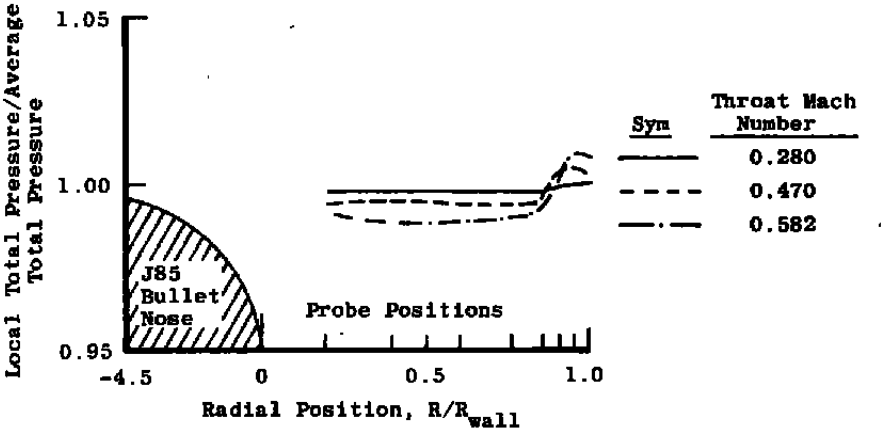

b. Screen Configuration A

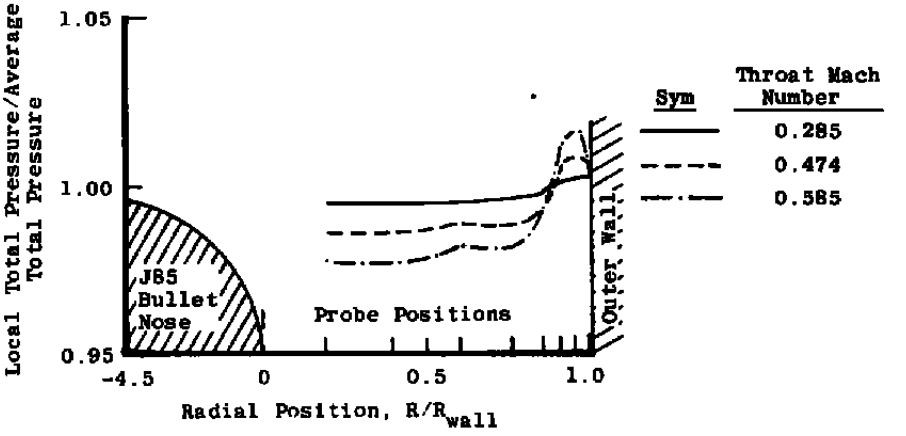

c. Screen Configuration B

Figure C-1. Engine face radial pressure profiles (98 percent of flow area) with subsonic venturi.

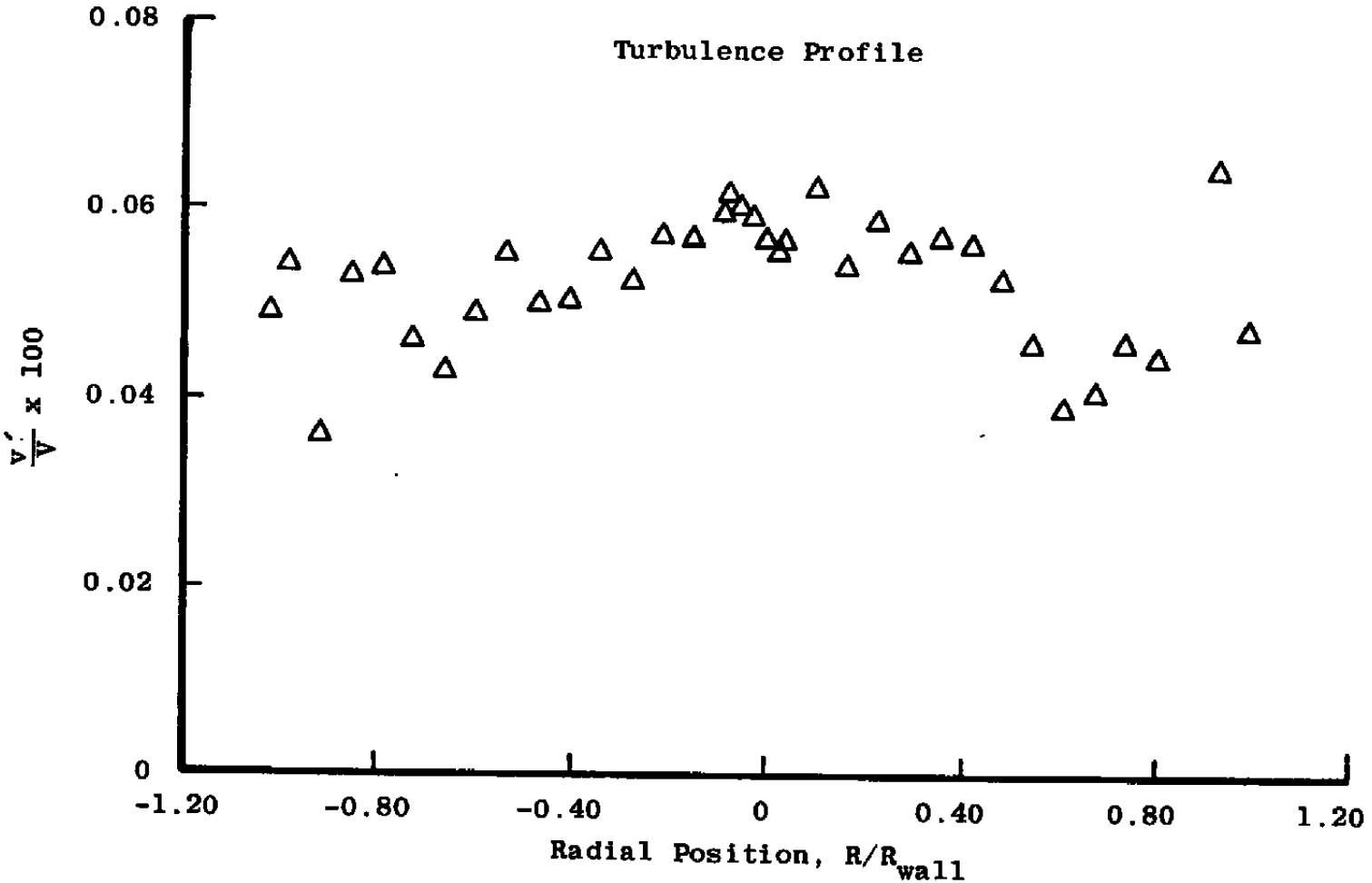

Figure C-2. Velocity profile screen and grid — Configuration A.

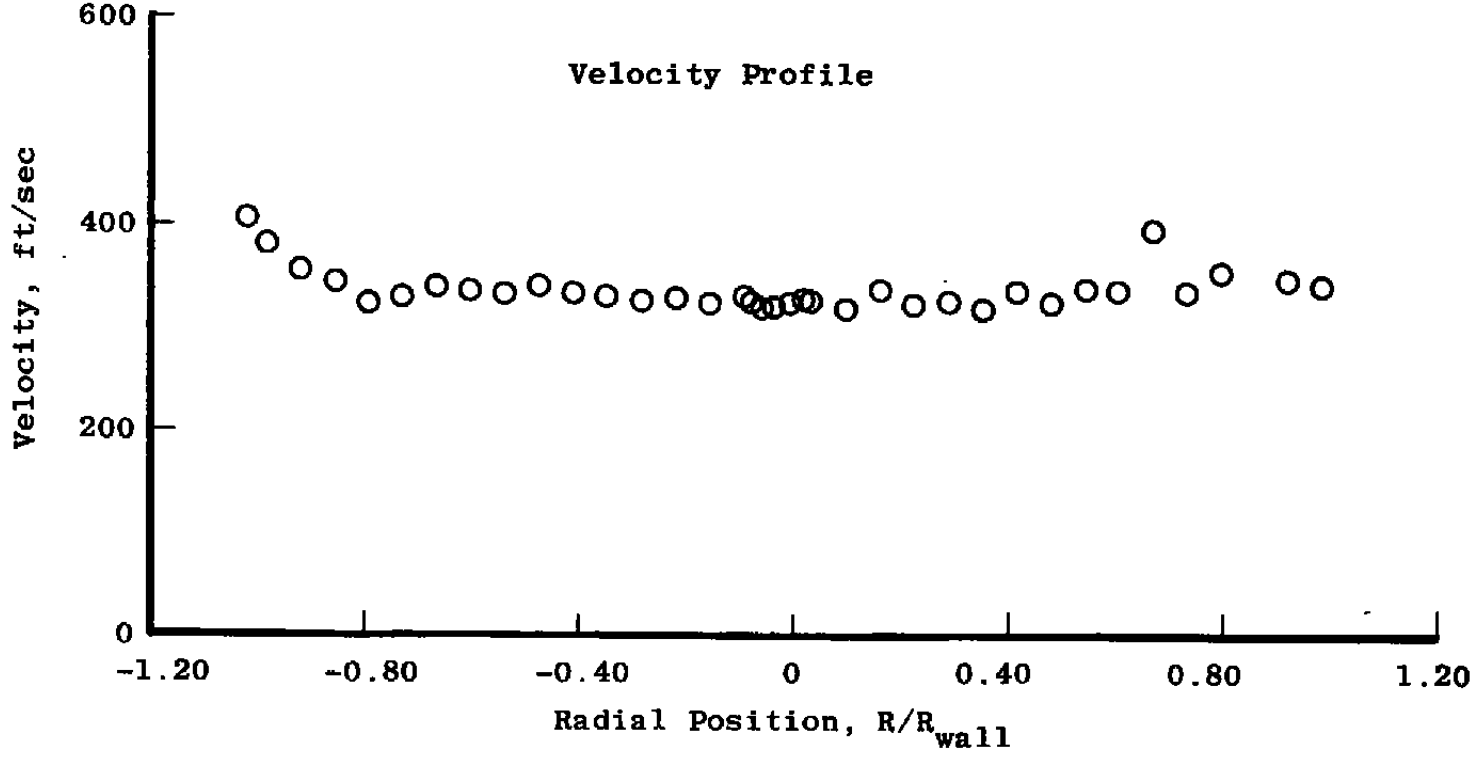

Figure C-3. Turbulence profile screen and grid — Configuration A.

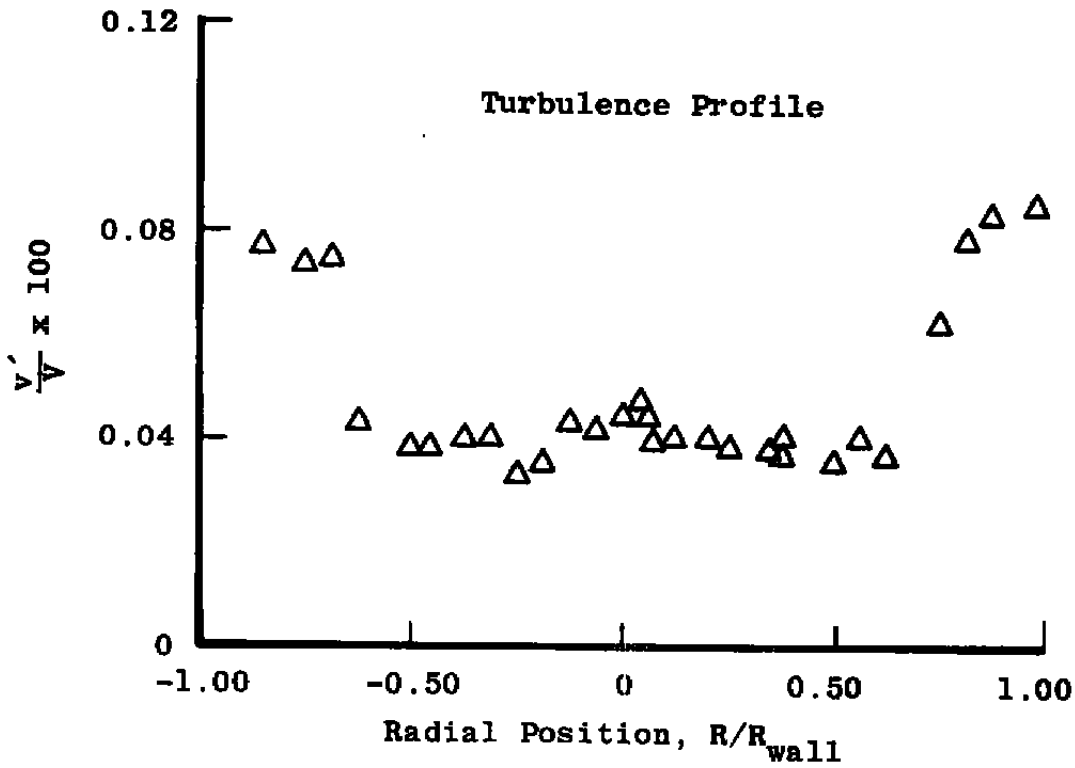

Figure C-4. Turbulence profile resulting from the safety support grid — no screen overlay.

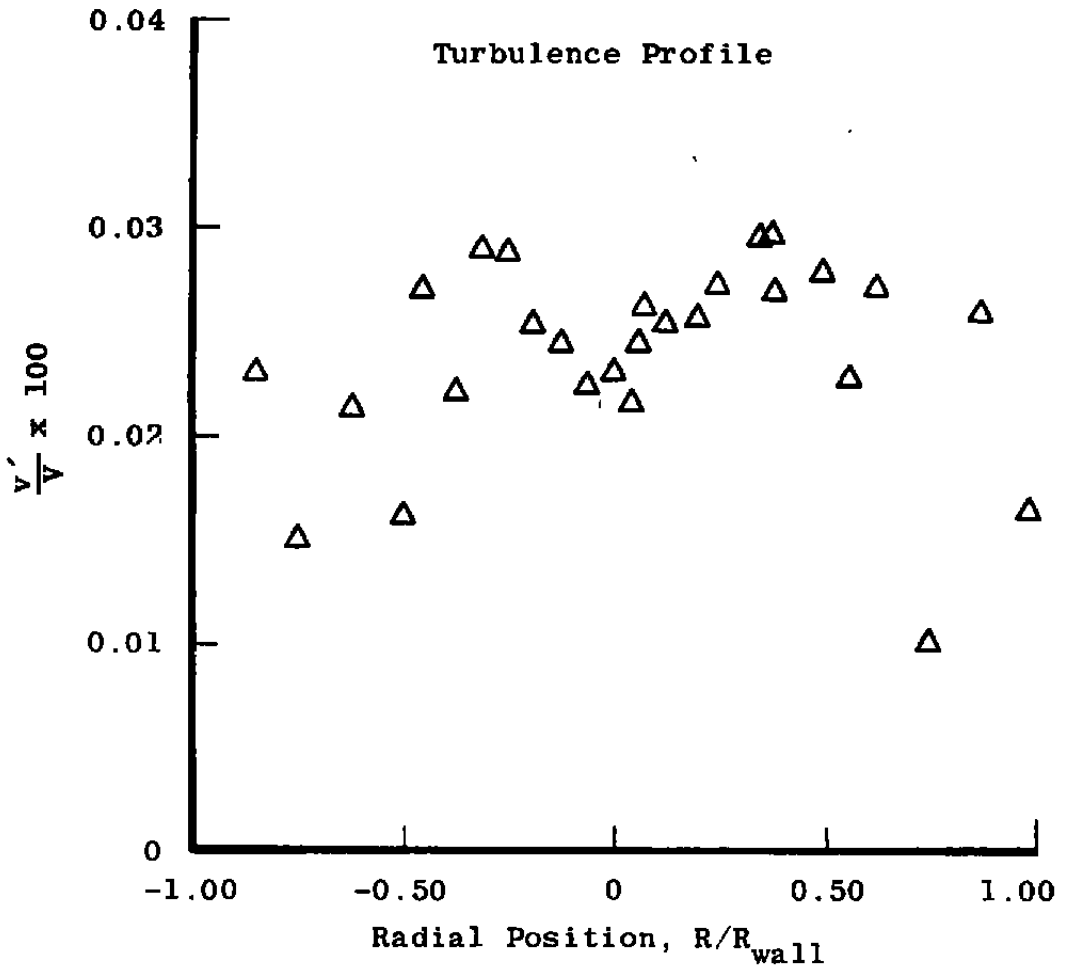

Figure C-5. Turbulence profile flow conditioner — Configuration B.

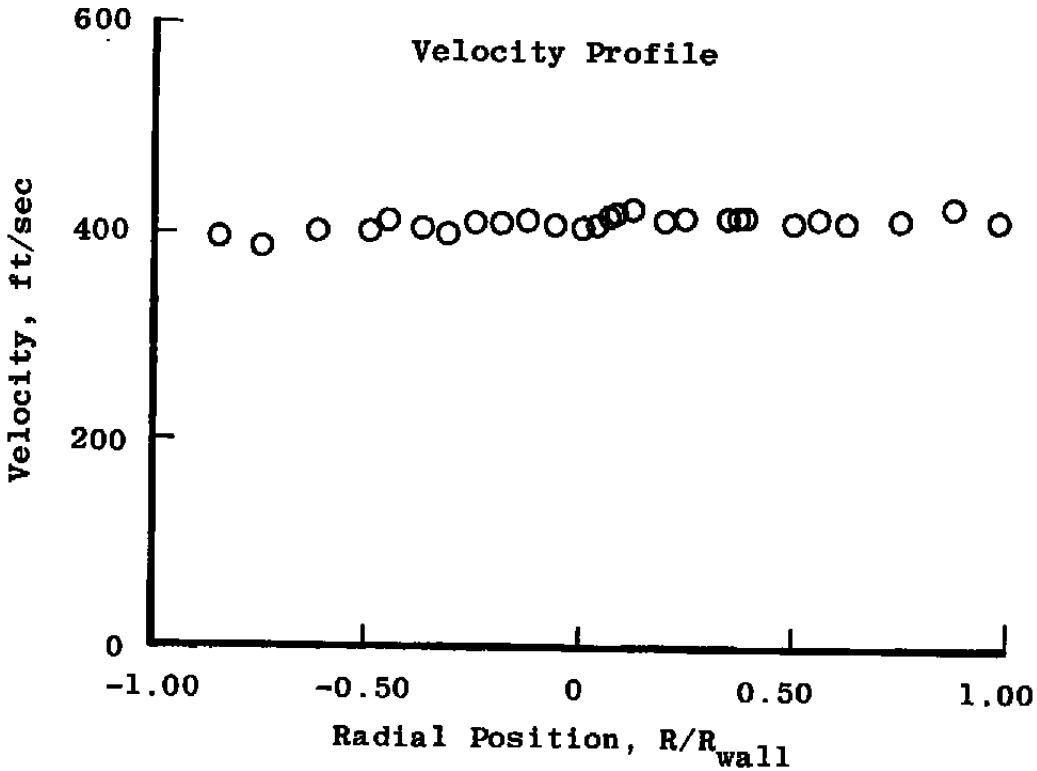

Figure C-6. Velocity profile flow conditioner — Configuration B.

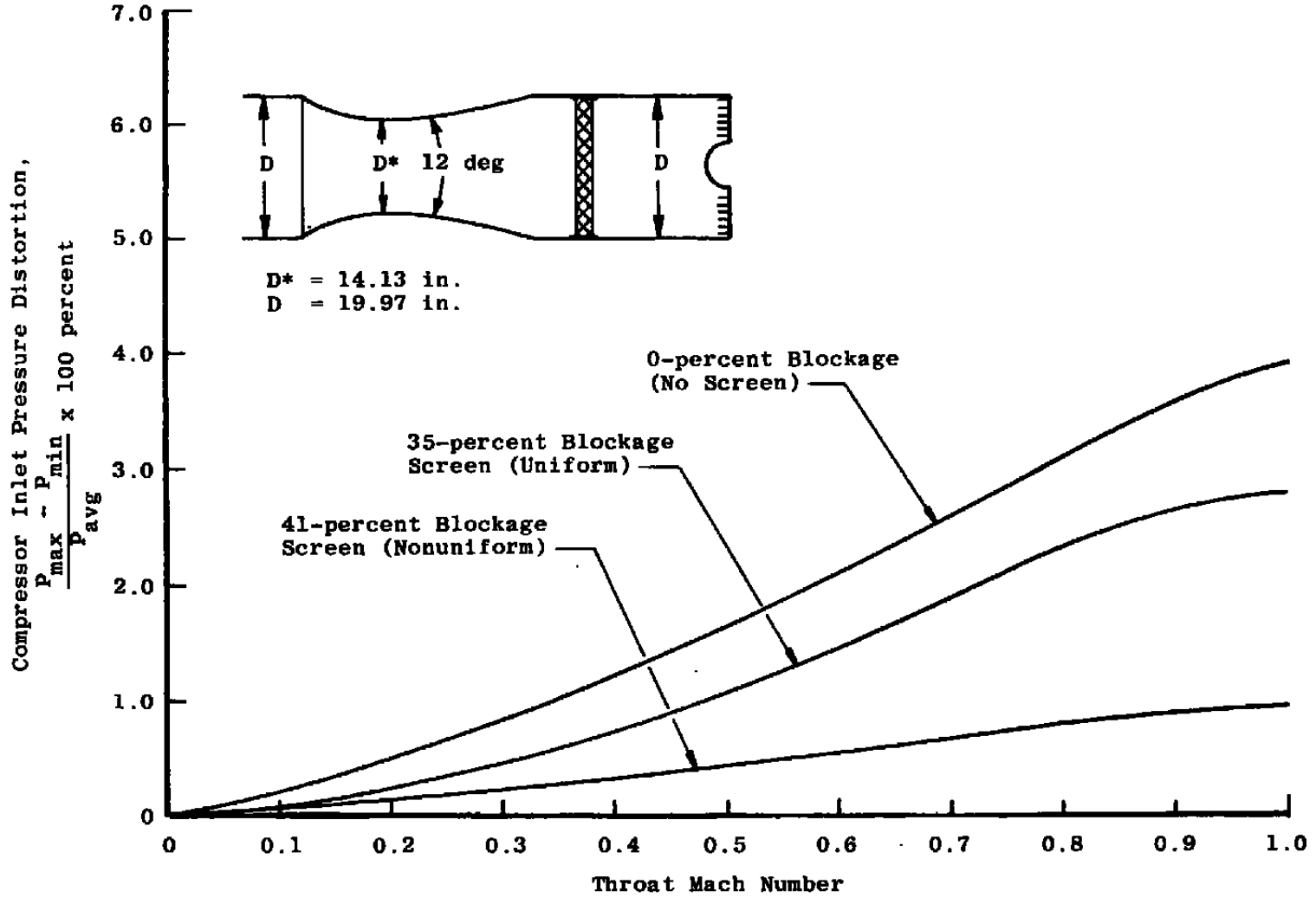

Figure C-7. Engine face total-pressure distortion (Ref. 17) (98 percent of flow area).

NOMENCLATURE

A	Area
D	Diameter
D*	Throat Diameter
DELW	Volumetric mass flow correction rate
L	Length of venturi throat
M	Mach number
P	Total pressure
POS	TETAS plug position
PS	Static pressure
R	Radius
R*	Throat radius
R_{wall}	Engine face radius
RG	Gas constant
T	Total temperature
t	Time
U	Measurement uncertainty
V	Mean velocity
v′	Fluctuating velocity
Vol	Volume
W	Mass flow rate
WAC	Corrected mass flow rate
β	Flow blockage area ratio
Δ	Difference
δ	Atmospheric pressure ratio

θ	Atmospheric temperature ratio
τ_o	Thermocouple reference time constant

Postscripts

1A, 1B, 3C, etc.	Instrumentation stations

Subscripts

avg	Area-weighted average
i	Initial
f	Final
max	maximum
min	Minimum
o	Outer wall
rms	Root mean square

Stations

1C	Sonic venturi flow straightener
1D	Sonic venturi plenum
1E	Sonic venturi throat
2B	Engine plenum
2C	Subsonic venturi throat
2D	TETAS inlet
2E	TETAS flow measurement plenum